



SCIENCE OF TSUNAMI HAZARDS

Journal of Tsunami Society International

Volume 31

Number 1

2012

THE SAMOA TSUNAMI OF 29 SEPTEMBER 2009

Early Warning and Inundation Assessment

Giovanni Franchello^{1*}, Alessandro Annunziato¹

¹European Commission, Joint Research Centre, Institute for the Protection and Security of the Citizen, TP 680, Via E. Fermi, 2749, I-21027 Ispra (VA), Italy

*Corresponding author, e-mail: giovanni.franchello@jrc.ec.europa.eu

ABSTRACT

On 29 September 2009 at 17:48:11 UTC, a large earthquake of magnitude 8 struck off-shore of the Samoa Islands and generated a large tsunami that destroyed several villages and caused more than 160 fatalities. This report first presents the characteristics of the earthquake and discusses the best estimations for the fault parameters, which are the necessary input data for the hydrodynamic tsunami calculations. Then, the assessment of the near-real time systems invoked by the Global Disasters Alert and Coordination System (GDACS)1 and the post-event calculations are performed, making comparisons with the observed tidal measurements and post-event survey. It was found that the most severely damaged locations are the Southern section of the Western Samoa Islands, Tutuila Isl in American Samoa and Niuatoputapu Isle in Tonga. This is in agreement with the locations indicated by the Red Cross as the most affected and with the results of the post-tsunami surveys. Furthermore, an attempt was made to map the inundation events using more detailed digital elevation models (DEM) and hydrodynamic modelling with good results. The flooded areas for which we had satellite images and post-tsunami surveys confirm the inundated areas identified correctly by the hydrodynamic model. Indications are given on the DEM grid size needed for the different simulations.

Key words: *GDACS; 2009 Samoa tsunami, tsunami propagation and inundation; early warning system; fault model; DEM assessment*

Science of Tsunami Hazards, Vol. 31, No. 1, page 19 (2012)

¹ <http://www.gdacs.org/>

1. INTRODUCTION

On 29 September 2009 at 17:48:11 UTC a large earthquake of magnitude 8 struck offshore of the Samoa Islands and generated a large tsunami that destroyed several villages and caused more than 160 fatalities.

The Joint Research Centre of the European Commission has developed an impact tsunami calculation system that is invoked automatically by the Global Disasters Alert and Coordination System (GDACS) when needed. During the Samoa event, the system was repeatedly activated when increasingly accurate information on the earthquake became available. Calculations are triggered when new parametric data (magnitude, depth and location) are published by seismological organizations (e.g. USGS, EMSC, GEOFON or others). The automatic system successfully identified the risk of a large event for the Samoa islands and its initial impact calculations were available online in less than 20 minutes after the earthquake event.

One day after the event, USGS published² the Global CMT Project Moment Tensor Solution for the earthquake and a day later the Finite Fault Model solution. The latter represents the best solution for the reconstruction of the initial fault form. This report shows the initial calculations, automatically performed by the JRC Tsunami Calculation System and the enhanced calculations performed in the days after the event, when the Finite Fault Model solution became available. Calculation accuracy is evaluated by quantifying the discrepancy between sea level measurements and the initial (near-real time) calculations, and more detailed follow-up calculations.

It is important, however, to underline that there are several types of calculations and each of them has its own merit and needs.

- *Grid scenario pre-calculations.* These are performed before an event for all likely tsunami scenarios (key parameters are epicentre and magnitude, more details will be presented in the next section) and stored in a database. General (conservative) assumptions on the fault mechanism are made. The nodalisation is deliberately rather coarse (cell size between 2 and 8 km) to shorten the calculation time and to limit the data volume. GDACS look up the scenario results in the database and use the estimated maximum sea level in the alerting logic.
- *Near-real time calculations.* They are automatically performed 15-20 min after the event as far as the information on the event became available. The fault mechanism at this stage is not well defined (therefore conservative assumptions must be made) and the position and depth of the earthquake epicentre are not precise at the beginning. The nodalisation is still rather coarse (as for the grid scenario calculation) to shorten the calculation time. The objective of these calculations is the identification of the likely locations under threat of inundation without intending to exactly predict the height in all these locations.
- *Post event calculations.* These are performed from 1-2 hours to several days after an event when more information becomes available on 1) the actual fault mechanism and 2) the measured tsunami waves and inundation zones. The simulation accuracy becomes more detailed, depending on the objective of the simulations and on the available DEM. The identified objectives are the following:

² <http://earthquake.usgs.gov/eqcenter/eqinthenews/2009/us2009mdbi/#scitech>

- *Alert assessment.* The objective here is to assess the tsunami predicted by the conservative grid scenario and near-real time calculations that use conservative fault sources and coarse grid sizing. This is necessary because it may be that no tsunami is associated with an earthquake, due to a very high depth or other fault mechanism for which the evaluated dislocation is negligible. For this assessment, the used grid size is typically in the range of 1 to 2 km.
- *Early run-up area identification.* The objective here is to identify more precisely the likely affected locations and try to estimate the run-up height and the potential inundation in the various coastal areas. The used grid size is on the order of 100 to 300m.
- *Inundation assessment.* If detailed DEM is available the inundation calculations can be performed. In this case the requested detail level is on the order of 10-to 30m-cell grid size. The results are affected by the precision of the available topography and bathymetry.
- *Risk assessment and risk management calculations.* They are performed before an event and are based on historical events. These calculations are aimed at preparing evacuation plans in case of tsunami. They are very much site specific and in general it is necessary to perform very detailed calculations reducing the cell size to 5 to 10m.

For the tsunami in Samoa, *post event calculations* have been performed in order to better understand the phenomena, identify the locations affected and obtain feedback to assess the near-real time calculations and evaluate the possibility to quantify the extent of inundation.

The analysis is conducted using three numerical codes: the *SWAN-JRC* code (Annunziato, 2007), which is the basis for the overall tsunami grid scenario calculations in support of GDACS; the *HyFlux2 JRC* code (Franchello, 2008), (Franchello, *et al.*, 2008), (Franchello, 2010), (Cruz, *et al.*, 2010) which is used for the inundation calculations; the *TUNAMI2* code (Imamura, Yalciner, & Ozyurt, 2006), to have another reference code.

The mentioned numerical codes solve the shallow water equations using different numerical methods: *SWAN-JRC* and *TUNAMI* use the finite difference method (FD) while *HyFlux2* uses the finite volume method (FV).

The *finite difference* method is largely used to model tsunami wave propagation and run-up. Models based on this scheme are usually less time consuming than those based on finite volumes. However, most of the FD codes present unphysical oscillations when dealing with flow discontinuities such as wetting and drying interfaces and bore formation.

- *The finite volume method has been developed in the past to simulate dam-break events and flash flooding and has been used recently also for tsunami modelling. The finite volume method is conservative in terms of mass and momentum and, if the dry/wet front is well modelled, the method is particularly suitable for run-up and inundation modelling.*

Science of Tsunami Hazards, Vol. 31, No. 1, page 21 (2012)

SWAN-JRC code is the numerical code implemented for the *Global Disaster Alerts and Coordination System (GDACS)*. GDACS has been jointly developed by the European Commission and the United Nations and combines existing web-based disaster information management systems, with the aim to alert the international community in case of major sudden-onset disasters and to facilitate the coordination of international response during the relief phase of the disaster. When a new event is detected by the seismological sources (USGS, EMSC), an evaluation of the importance of the event from a humanitarian point of view is performed. In case of an earthquake event occurring under water and of magnitude greater than 6.5, the JRC Tsunami Assessment Tool is invoked and a new calculation is requested. The SWAN-JRC model solves the shallow water equations by the finite difference numerical scheme based on the Mader code (Mader C., 2004).

The SWAN-JRC code estimates also the fault length, height and direction to determine the initial water displacement. The code initializes the calculation space, performs the travel time propagation calculation, verified at each step if there are locations reached by the wave and thus updates the visualization and animation files. For early warning purposes the model can run automatically and will publish the results in the GDACS web site.

TUNAMI code consists of several sub-codes:

- (a) TUNAMI-N1, linear theory with constant grids.
- (b) TUNAMI-N2, linear theory in deep sea, shallow-water theory in shallow sea and run-up on land with fixed grids.
- (c) TUNAMI-N3, linear theory with varying grids.
- (d) TUNAMI-F1, linear theory for propagation in the ocean in the spherical coordinates.
- (e) TUNAMI-F2. linear theory for propagation in the ocean and coastal waters.

In this analysis TUNAMI-N2 has been used. The TUNAMI code package is included in the SWAN-JRC suite and therefore the results can be easily produced within the same environment as the SWAN code.

HYFLUX2 code has been developed to simulate severe inundation scenarios due to dam break events, flash floods and tsunami-wave run-up. The model solves the conservative form of the two-dimensional shallow water equations using a finite volume method. The interface flux is computed by a Flux Vector Splitting method for shallow water equations based on a Godunov-type approach. A second-order scheme is applied to the water surface level and velocity. Physical models are included to deal with bottom steps and shorelines. The second-order scheme together with the shoreline-tracking method makes the model well balanced in respect to mass and momentum conservation laws, providing reliable and robust results. In HYFLUX2, numerical stability is ensured under the Courant-Friedrich-Levy (CFL) criteria (Franchello, 2010).

In addition, HYFLUX2 is included in the suite of codes that can be invoked by the SWAN-JRC suite, thus enabling an easy comparison of the code results.

NOAA-MOST code. The MOST package (Titov, *et al.*, 2005) is a suite of numerical simulation codes capable of simulating three processes of tsunami evolution: earthquake deformation, transoceanic propagation and inundation.

MOST Tsunami modelling proceeds in three distinct stages:

- A Deformation Phase generates the initial conditions for a tsunami by simulating ocean floor changes due to a seismic event.
- A Propagation Phase propagates the generated tsunami across deep ocean using Nonlinear Shallow Water (NSW) equations.
- An Inundation Phase simulates the shallow ocean behaviour of a tsunami by extending the NSW calculations using a multi-grid “run-up” algorithm to predict coastal flooding and inundation.

The tsunami generation process is based on a fault plane model of the earthquake source (Okada, 1985), which assumes an incompressible liquid layer on an underlying elastic half space to characterize the ocean and the Earth’s crust. The implementation of this elastic fault plane model (Titov, 1997) utilizes a formula for static sea-floor deformation to calculate the initial conditions required for subsequent computations of tsunami propagation and inundation.

The near-real time calculations performed by NOAA considered the best fitting scenario used at the moment of an event. NOAA’s Pacific Marine Environmental Laboratory (PMEL) forecast system combines real-time seismic and tsunami data with a forecast database of pre-computed scenarios. The database model scenarios for unit sources consist of fault blocks of 100 km along strike and 50 km down dip. The model requirement in this case is similar to retrospective studies: the solution must provide the best fit to the observations (Titov *et al.*, 2005) and use seismic or DART scaling factors to fit the data. The use of these scaling laws may be inadequate for complex events resulting in forecasting errors (Weinstein S., 2008).

NOAA-MOST initial conditions are adjusted by direct comparison with the Deep-ocean Assessment and Reporting of Tsunamis (DART) buoys stations available records, in order to estimate correctly the source parameters that better represent the results (tsunami forecast)³.

Commonly, most of the numerical tsunami models use nested computational grids from coarse to high-resolution, to get more detail into the area of interest, i.e., the coastal flooding and inundation is commonly simulated by extending propagation calculations with such a nested grid approach.

The most common procedure to track movements of the shoreline (Imamura, *et al.*, 2006) is the moving boundary treatment. Run-up is calculated with nonlinear computations.

Science of Tsunami Hazards, Vol. 31, No. 1, page 23 (2012)

³ NOAA-MOST results are accessed online through an agreement between NOAA and JRC.

HYFLUX2 uses a shoreline tracking method to model the interface between dry and wet zones (Franchello, 2010). HYFLUX2 inundation 2D scheme has been designed to identify the shoreline as an intersection between two planar surfaces, which describe the bottom, and the water free surface. Mass conservation is always realised during the wetting/drying processes. With this method a cell can be partially wetted, i.e. the fraction of cell that is wetted is a result of the proposed shoreline tracking methodology.

Other FV models have realized a preservation of mass conservation during dry/wet processing by reconstructing the bottom topography (Audusse, *et al.*, 2004), (Brufau, *et al.*, 2003), (Marche, 2005), (Liang, 2010).

Another way to describe the wet/dry moving front and inundation process is the adaptive grid approach, which is studied in detail in (Liang, 2004), and (Liang, 2010).

In the TUNAMI-N2 code, like in other FD models, a numerical algorithm is needed to determine if the total water depth is high enough to flood the neighbouring dry cells (land) and hence to move the shoreline. Momentum equations are used to update the volume in the wet cells only. When the water surface is rising, the volume flux is no longer zero and the shoreline moves one grid point in the onshore direction.

2. DESCRIPTION OF THE TSUNAMI EVENT

2.1. Tectonic Summary

In order to perform correct tsunami simulations of the 29 September 2009 Samoa earthquake, it is necessary to take into account the tectonic setting and seismicity of Samoa and its surrounding area. It is important to analyse the entire scenario of effects by carrying out a sensitivity analysis on earthquake parameters in the form of epicentre, depth, fault length, fault width, slip distribution and fault mechanism (Annunziato, 2009).

The earthquake occurred as part of a clustering of major seismic activity in the north of Tonga Trench (TT) which may have reflected a reactivation of all major plate boundaries in the region (Pelletier, Calmant & Pillet, 1998).

The Tonga Trench is located in the Pacific Ocean and is 10882 meters (35702 ft) deep at its deepest point, known as the Horizon Deep. It is a deep canyon on the edge of the Pacific Plate. The region has a complex tectonic regime and very high level of seismic activity related to the compression motion between the Pacific and Australian Plates (Pelletier, Calmant, & Pillet, 1998).

The Pacific tectonic plate dives beneath the Australian plate at a rate of almost a centimetre a year, making the area one of the most active earthquake regions in the world. Earthquakes occur within the Pacific plate on both sides of the trench. The trench and associated faults are forming as the Pacific Plate moves westward, sinking beneath a complex series of smaller plates on the edge of the Australian Plate. There have been around 30 quakes of magnitude 7.0 or more along this trench since 1900⁴. The Figure 1 shows the location of the earthquake in relation to the Samoa islands.

Science of Tsunami Hazards, Vol. 31, No. 1, page 24 (2012)

³NGDC Tsunami Runup database, <http://www.ngdc.noaa.gov/nndc/struts/form?t=101650&s=167&d=166>

⁴ Deep-ocean Assessment and Reporting of Tsunamis, <http://nctr.pmel.noaa.gov/Dart/>

⁴

<http://www.un.org.au/files/files/Samoa%20Tonga%20Tsunami%20OCHA%20SitRep%20No%206%206%200ct%2009.pdf>

⁴ <http://earthquake.usgs.gov/regional/ncic>

In an extensive study performed on year 1980 (Pararas-Carayannis, et al., 1980) about 60 tsunamis - generated by earthquakes in the Pacific Ocean - have located the Soamoa Islands. The 2009 tsunami under analysis was very similar to the one on June 26, 1917.

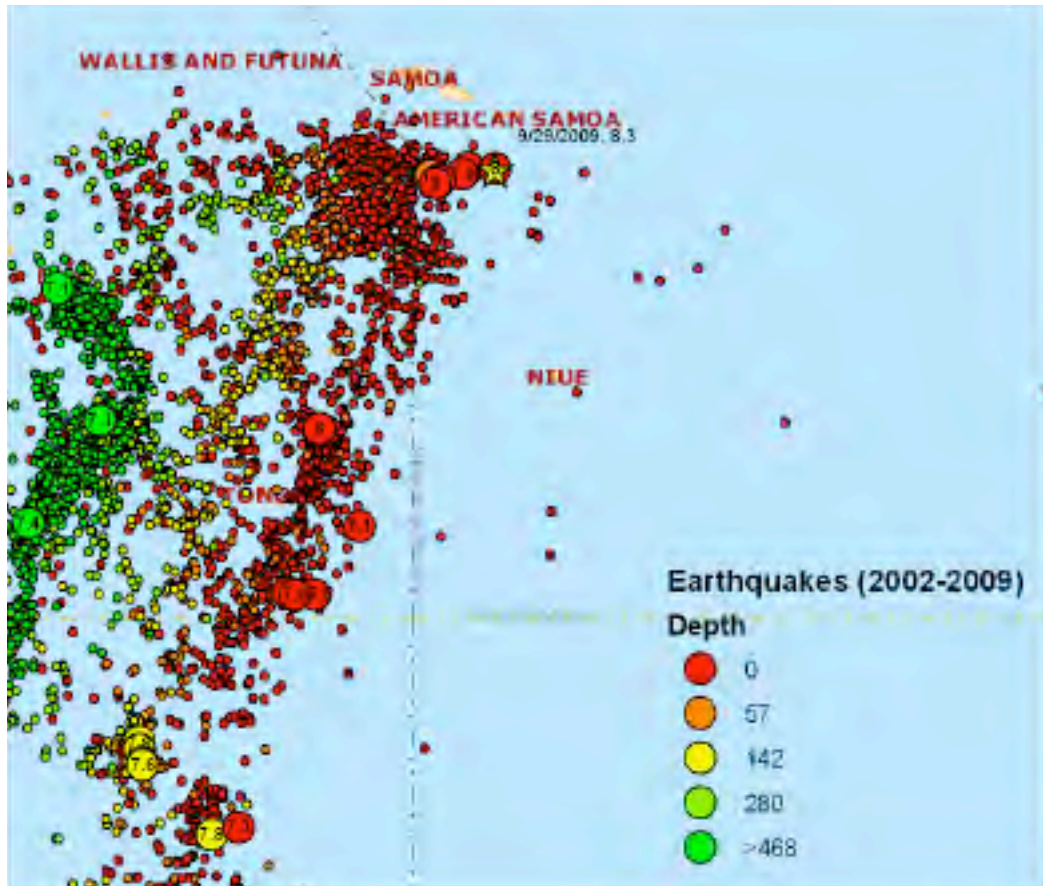


Figure 1 - Distribution of the historical earthquakes (dots) and epicentre of the 29 September 2009 Samoa earthquake (star)

2.2 Available measurements

Several in-situ sensors are located in the area, but not all were functioning during the event. The closest to epicentre online measurement points, against which the calculations will be compared, are shown in Figure 2.

According to the tsunami travel time both DART buoys should have been reached in about 1h and the tidal measurements between 15 and 25 minutes after the event.

A negative initial wave was recorded by 3 sensors (51425, Apia and Pago Pago, (see Figure 3, figure 5, Figure 6) which is consistent with the proposed fault mechanism (see next chapter). The sensor on the North – Northeast side shows a negative section; while 51426 shows (Figure 4) an initial positive section which could indicate that a higher positive section should be present in the Southern part of the fault.

There are several other measurement points available in the Pacific Ocean that can be useful to estimate the arrival time, but the ones indicated are the most relevant to analyse the tsunami phenomenon with acceptable detail.

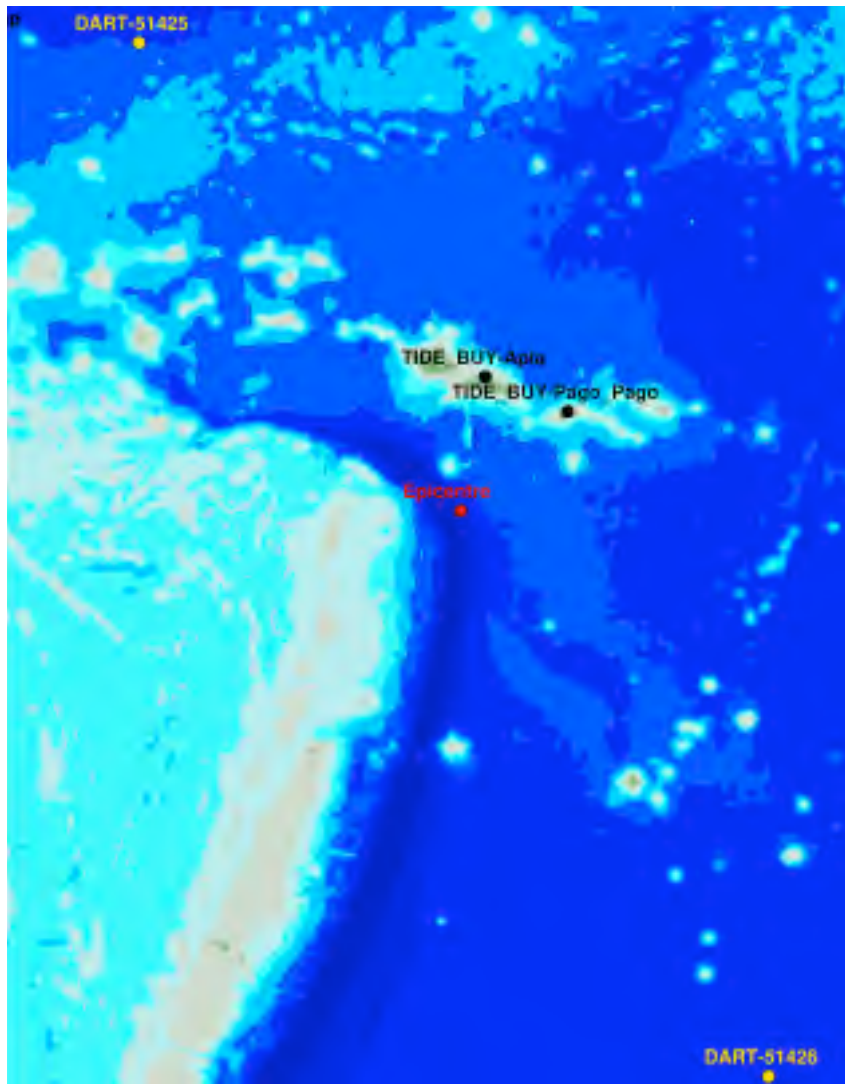


Figure 2 - Online measurements

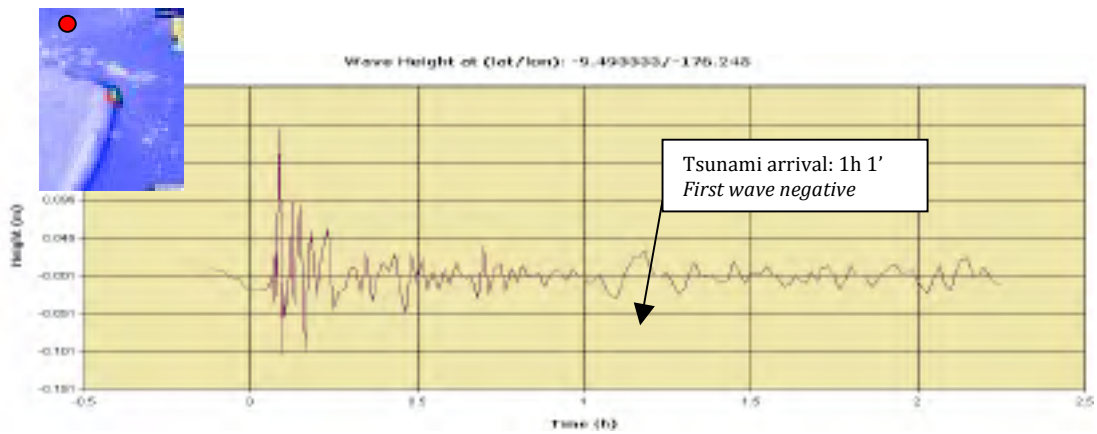


Figure 3 - DART Measurement 51425

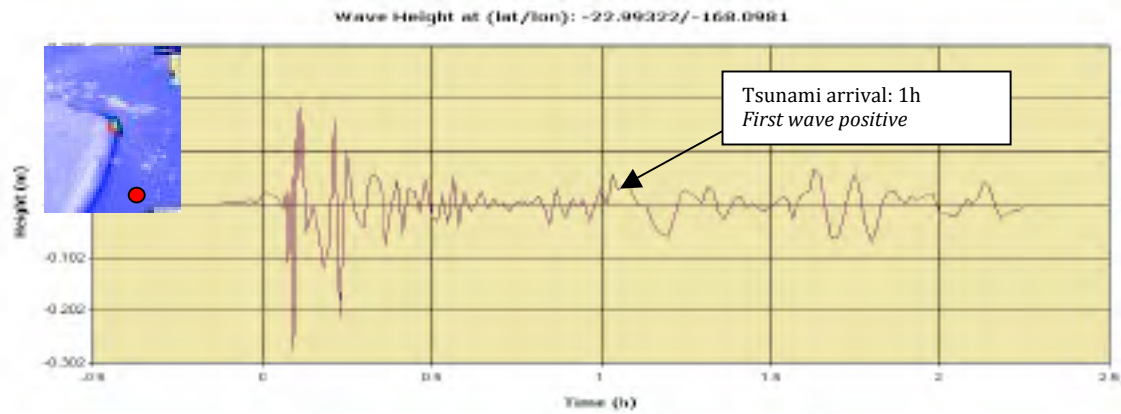


Figure 4 - DART Measurement 51426

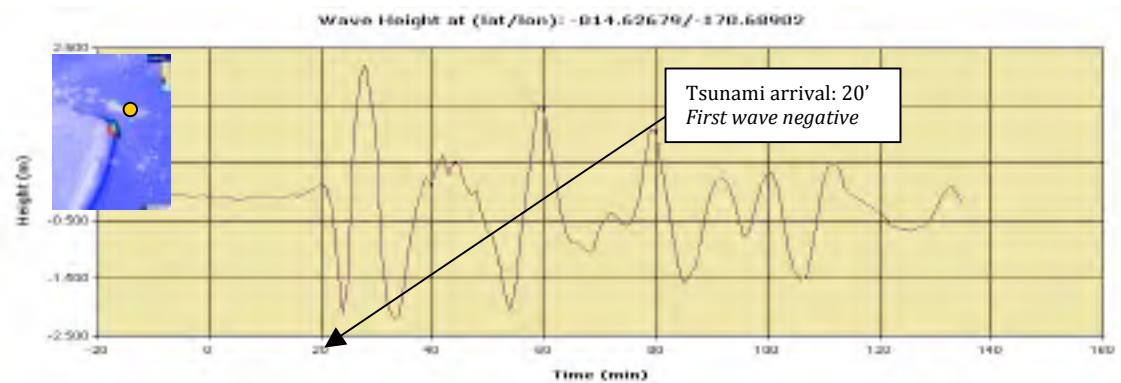


Figure 5 - Tidal measurement in Pago-Pago

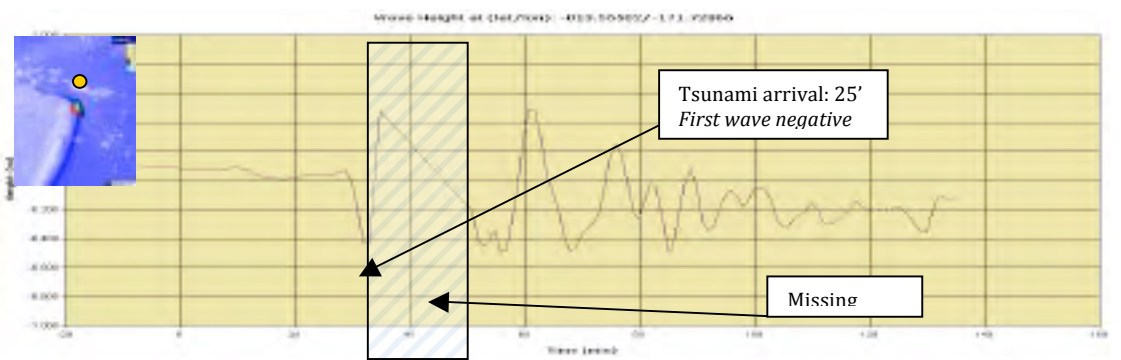


Figure 6 - Tidal measurement in Apia

The conditions of the tide at the time of the tsunami were in the descending part (Figure). In this location and this period of the year, the tidal height does not show large variations, about 0.5m between minimum and maximum. Post-tsunami survey measurements on the run-up height 5 and damage maps performed using satellite images on the inundated area⁶ became available on the web some weeks after the event.

Science of Tsunami Hazards, Vol. 31, No. 1, page 27 (2012)

⁵ <http://www.ngdc.noaa.gov/nndc/struts/form?t=101650&s=167&d=166>

⁶ http://unosat.web.cern.ch/unosat/asp/prod_free.asp?id=125

http://unosat.web.cern.ch/unosat/asp/prod_free.asp?id=126

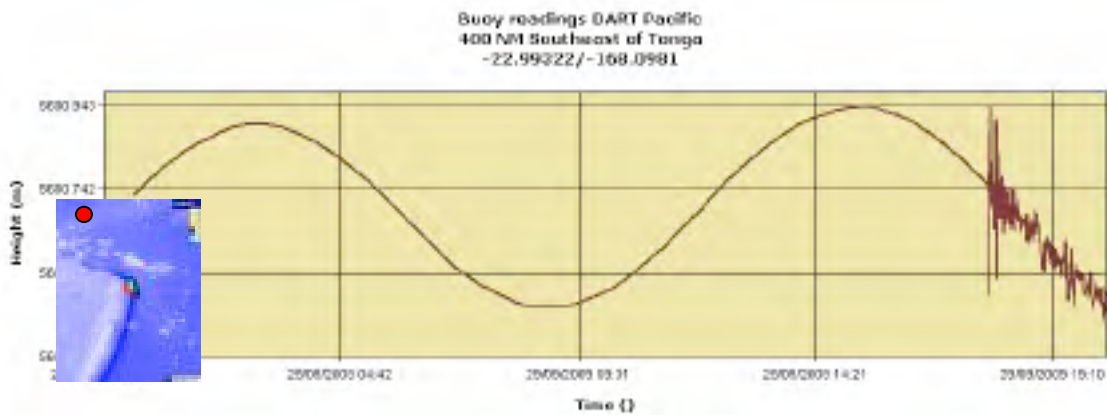


Figure 7 - DART Measurement 51425, long range, tidal data

Most of the post-tsunami survey measurements were done in Tutuila Island (American Samoa), where 34 fatalities were recorded, while on Opolu Island – with 149 fatalities – only the buoy measurement is available. On Niauatoputapu Island – with 9 fatalities – no measurements were recorded in the NGDC database, but a field survey done 2 months later recorded a maximum run-up of 22 m (EERI, 2010). Damage maps performed using satellite images (see Figure 8 and Figure 9) are available for Saval'i & Upolu Islands (Samoa) and for Tutuila Island (American Samoa).



Figure 8 - Overview of tsunami damage on Tutuila Island



Figure 9 - Overview of tsunami damage on Savai'i & Upolu Islands

Table 1 - Post-tsunami survey measurements. Type: 1 = Eyewitness, 5 = Post-tsunami Survey, 2 = Tide-gauge, 3 = Deep ocean gauge, 6 = Atmospheric Wave, 7 = Seiche

Tsunami Runup Location				Tsunami Runup Measurements					Tsunami Runup Location Effects	
Name	Latitude	Longitude	Distance from Source	Travel Time		Max Water Height	Type	Per	Lst Mtn	Deaths Num
				Hrs	Min					
NIUATOPUTAPU	-15.95	-173.75	184				1			9
AMANAVE, AMERICAN SAMOA	-14.333	-170.829	187			7	5			
POLOA, AMERICAN SAMOA	-14.322	-170.833	188			16.3	5			
LEONE, TUTUILA I, AMERICAN SAMOA	-14.344	-170.791	189			5	5			
UPOLU, APIA	-13.817	-171.75	190		21	0.78	2	8	R	149
FAGATELE BAY, AMERICAN SAMOA	-14.37	-170.764	190			5	5			
VAITOGI, AMERICAN SAMOA	-14.359	-170.735	193			4	5			
PAGO PAGO, AMERICAN SAMOA	-14.283	-170.683	203	0	11	2.16	2	8	R	34
PAGO PAGO, AMERICAN SAMOA	-14.281	-170.674	203			7	5			
FAGAITUA, AMERICAN SAMOA	-14.28	-170.612	209			4	5			
AMOULI, AMERICAN SAMOA	-14.278	-170.583	211			3	5			
ONENOA, AMERICAN SAMOA	-14.257	-170.58	213			4	5			
TULA, AMERICAN SAMOA	-14.258	-170.564	214			7	5			
FAGAMOLA, AMERICAN SAMOA	-14.249	-169.504	311			12	5			
NUKUALOFA (NUKU'ALOFA)	-21.133	-175.167	707	0	59	0.15	2	10		
D51425 BPR, 370 NM NW Of APIA	-9.493	-176.245	805			0.04	3			
D51426 BPR, 400 NM SE OF TONGA	-22.993	-168.098	934			0.05	3			

Separate focus maps are included, highlighting damage sites identified from post-disaster satellite imagery collected from 30 September to 4 October 2009. Damage identification was restricted by the partial coverage and spatial resolution of the imagery, as well as by cloud cover. It is probable therefore that damage estimates have been underestimated. This assessment was a preliminary analysis not yet validated in the field when the report (UNITAR/UNOSAT, 2009) was written.

3. SIMULATION METHODOLOGY AND BOUNDARY CONDITIONS

The tsunami simulations depend strongly on: a) the initial fault mechanism; b) the hydraulic conditions (DEM, cell size). It is also important to point out that the earthquake information available immediately after the event were only epicentre, magnitude and depth. All these estimated quantities may change significantly in time due to progressive improvement of the seismological parameters. The day after the event the fault mechanism was identified and two days later USGS published the finite fault model solution, which is the best characterization of the fault available at the moment.

The choice of the tsunami source is usually a complicated issue because it requires good knowledge of the earthquake parameters such as epicentre, depth, fault length, fault width, slip distribution and rupture mechanism. It is assumed that the tsunami is generated by co-seismic displacement of the sea floor. Thus, the initial condition for the modelling of the expected tsunami in the region is assumed to coincide with the vertical co-seismic displacement of the sea bottom induced by the earthquake. The initial conditions are one of the major factors that affect the wave propagation and the resulting run-up amplitudes along the coast. Different approaches can be used to calculate the initial conditions from the motion of the fault.

The first approach is to evaluate the Earth deformation caused by the earthquake and impose an initial water level as proposed by Ward (Ward, 2002). This approach gives the initial water level increase by using the empirical relationships between the magnitude of the earthquake and fault length and width.

The second one was developed by Okada (Okada, 1985). This algorithm calculates the distribution of co-seismic uplift and subsidence by using the epicentre of the earthquake, fault strike, fault dip, fault rake and amount of average displacement on the fault.

The third approach is to use the fault and the direction of slips by separating the fault plane into sub-faults. In order to reveal the rupture process of the fault with this approach, USGS uses GSN broadband waveforms downloaded from the National Earthquake Information Centre (NEIC) waveform server⁷. They analyse teleseismic broadband P waveforms, broadband SH waveforms and long period surface waves selected based on data quality and azimuthal distribution. Waveforms are first converted to displacement by removing the instrument response and then used to constrain the slip history based on a finite fault inverse algorithm (Ji, Wald, & Helmberger, 2002).

The earthquake parameters, fault mechanism solutions and slip distribution cross-section of the fault model – which are available after the earthquake from the different organizations – are given respectively in fault model – which are available after the earthquake from the different organizations – are given respectively in Table 2 and Table 3. The mechanism solutions show an almost normal fault, on a plane striking roughly parallel to the Tonga Trench axis, with seismic moment of 1.82×10^{28} dyne cm.

Science of Tsunami Hazards, Vol. 31, No. 1, page 30 (2012)

⁷ http://earthquake.usgs.gov/earthquakes/eqinthenews/2009/us2009mdbi/finite_fault.php

Table 2 - Earthquake parameters (USGS/NEIC)

Magnitude (Mw)	8.0
Date and Time	29, September 2009 at 17:48:10 UTC
Location	15.509°S, 172.034°W
Depth (km)	18
Region	Samoa Island Region

In the following sections we will show the fault mechanisms adopted for the various phases and will compare them.

3.1 Fault mechanism and hydraulic initial condition

For the definition of the hydraulic initial condition it is assumed that the bottom floor Earth deformation is instantaneously transmitted to the water. Thus the initial water level field is initialized with the bottom deformation.

The near-real time calculations were performed using the JRC fault model (based on the Ward approach), which should be considered as an upper bound or worst case. Several calculations were automatically requested by the early warning system (see Table 6) until the epicentre was better identified (see previous chapter). The final case has been performed with the following parameters:

- L=158 km, W=44 km, Strike=318.4, Form Cosinusoidal, all positive, Slip=3.16m

The JRC fault model (see Figure 10, left assumes a cosinusoidal shape all positive, in order to maximize the impact. The model assumes a standard earthquake depth of 5 km, and applies a scaling factor for the real depth. For a depth of 18km, the depth factor is 0.8. Thus, the calculated wave height of 3.16m is reduced to 2.5m.

Other near-real time calculations during the event were those performed by NOAA⁸ with the MOST code (Titov, *et al.*, 2005). They found that the best solution for the current fault (as compared with the DART measurements), was obtained using the unit sources ntsza34 plus the ntszb34 solution, both multiplied by the factor 3.96 (see Figure 10 – Fault models: JRC left, NOAA, right). It should be remembered that every NOAA unit fault source corresponds to a 100 km x 50 km fault of elevation 1m (e.g. corresponding to a magnitude of 7.5); thus it is necessary to multiply by some factor to take into account the magnitude difference.

⁸ <http://nctr.pmel.noaa.gov/propagation-database.html>

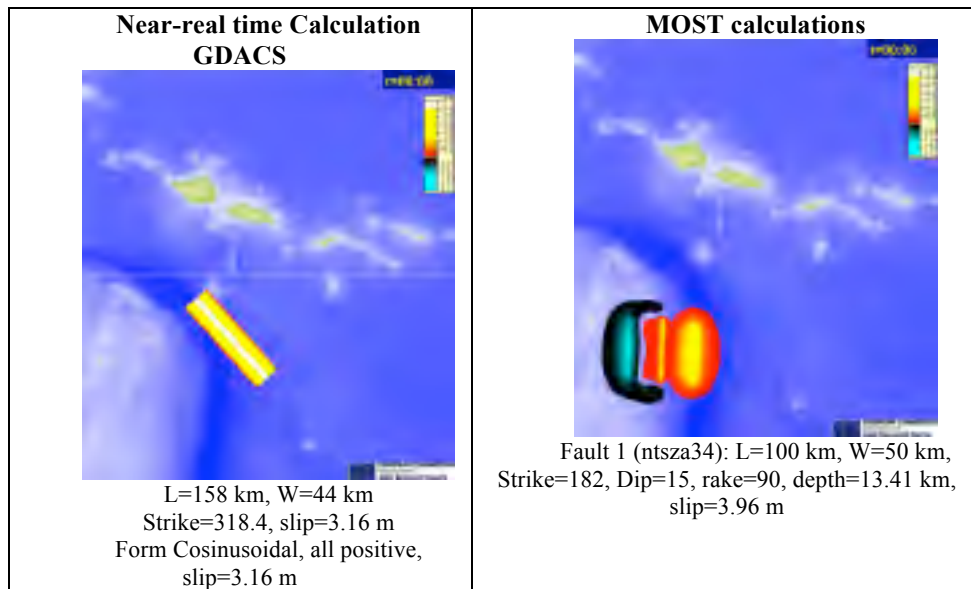


Figure 10 - Fault models: JRC left, NOAA right

According to the fault mechanisms published by USGS the day after the event, two possible solutions can be analyzed; the USGS solution and the Harvard one. They differ for the location and mostly for the strike angle (more vertical in the Harvard case).

The parameters in Table 3 have been included in the Okada model (Okada, 1985) in order to set up the initial deformation.

Table 3 - Fault mechanism solutions

Time 17:48:10.57	Lat/L	Mag	Strike	Dip	Rake	Depth
	on	(Mw)				(km)
USGS Centroid Moment Tensor Solution	- 15.418/- 172.005	8.0	345	46	-61	10
Harvard Global CMT Project Moment Tensor Solution	- 15.195/- 171.9	8.1	7	71	-64	12

Two days after the event the Finite Fault Model solution was published by USGS. The hypocenter adopted was the USGS one (Lon. =-15.60 deg.; Lat.=-172.30 deg.).

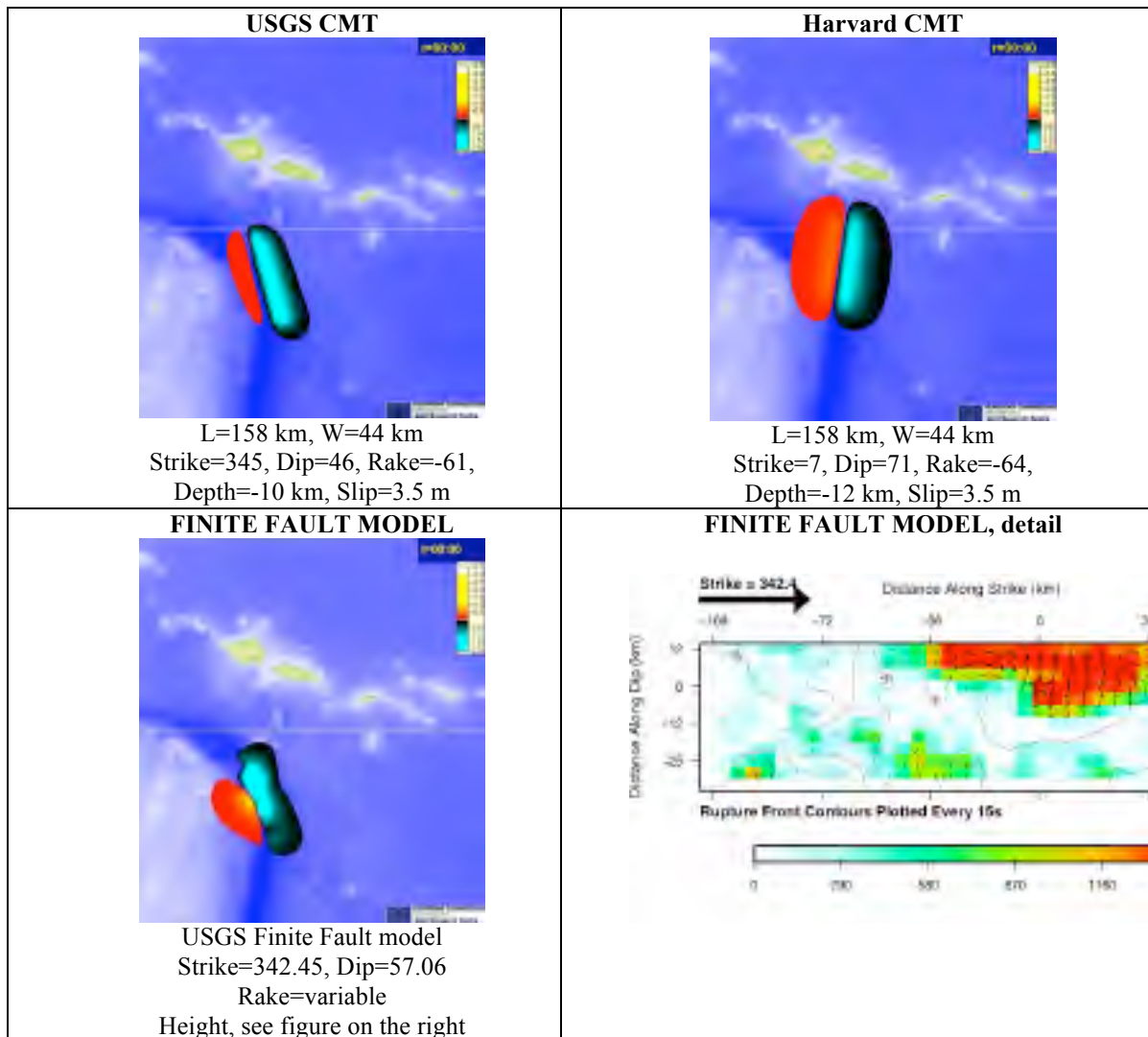


Table 4 - Different sources for post-event calculations. The best “simple” solution is the one proposed by CMT USGS.

The result of this procedure is a series of 432 individual sources of 5 km by 4 km; all at strike 342.45 and dip 57.06. All fault planes have their own rake and slip. Combined, the sources produce an initial deformation as shown in the previous figure, which indicates that the best “simple” solution is the one proposed by CMT USGS.

In order to evaluate the effect of each solution on the wave height estimates, it is necessary to run simulations for the various source solutions. It may be anticipated however that, contrary to the adopted initial condition for the near-real time calculation (cosinusoidal shape a ll positive), all the solutions show a negative section on the Northeast side.

Most of the calculations have been performed using as initial conditions the Finite Fault model because it is considered to be the best one, as confirmed by sea level measurements.

About one year after the event (Lay, et al., 2010), further detailed analysis of the seismic information indicated that the tsunami could be enhanced by an additional doublet triggered 2 minutes after the initial normal fault event (magnitude 8). This doublet corresponds to a second earthquake of magnitude 8.

Another study published at the same time (Beaven, et al., 2010), proposed a fault model consisting of a slow thrust event of magnitude 8 which triggered several minutes after a normal fault (outer rise) event of magnitude 7.9. The analysis was based on using GPS measurements, field surveys in Niuaotupapu Island (close to the epicentre) and DART measurements. However, the objectives of this paper is to understand what the accuracy is of the tsunami early warnings triggered by the fault models data available from a few minutes to a few days after the event: for this reason these latter analyses performed one year after the event have not been included in the present study.

3.2 Digital elevation model

The available Digital Elevation Models (DEM) used for the simulations are listed in Table 5.

Table 5 - Bathymetry and Topography used for the simulations

Source	Grid size	Bathymetry	Topography	Coverage
ETOPO1 Global Relief Model 9	1'	yes	yes	World
SRTM30 PLUS Global topography (v 5.0)¹⁰	30''	yes	yes	World
GEBCO Global Topography¹¹	30''	yes	yes	World
SRTM DTED® Level 1 (3 arc second)¹²	3''	NO	yes	World
NOAA - AS 3 arc-second Pago Pago¹³	3''	NO	yes	Pago Pago
NOAA - AS 1/3 arc-second Pago Pago¹⁴	1/3''	yes	Yes	Pago Pago.

The most reliable data sources for which both bathymetry and topography are available worldwide are SRTM³⁰ PLUS¹⁰ and GEBCO¹³. For the inundation simulations in Tutuila Island^{15,16} the DEM developed by NOAA (Lim, et al., 2009) have been used. A sensitivity analysis with respect to the available DEM is described in the next section.

4. GDACS ASSESSMENT

The Global Disaster Alert and Coordination System (GDACS) aims at alerting the international humanitarian response community to impending disasters that will require international response. GDACS consists of an automatic alerting system (sending SMS, email and fax alerts to around 10000 users) and a restricted website for professional responders (the Virtual OSOCC).

Science of Tsunami Hazards, Vol. 31, No. 1, page 34 (2012)

⁹ <http://www.ngdc.noaa.gov/mgg/global/global.html>

¹⁰ http://topex.ucsd.edu/WWW_html/srtm30_plus.html

¹¹ http://www.bodc.ac.uk/data/online_delivery/gebco/










¹² <http://edcns17.cr.usgs.gov/EarthExplorer/>

¹³ <http://www.ngdc.noaa.gov/dem/showdem.jsp?dem=Pago Pago&state=AS&cell=3 arc-second&vdat=MHW>

¹⁴ <http://www.ngdc.noaa.gov/dem/showdem.jsp?dem=Pago Pago&state=AS&cell=1/3 arc-second&vdat=MHW>

After the Samoa event, seismological institutions published more accurate data, which triggered new impact evaluations (see Table 6). The first data was received from the Pacific Tsunami Warning Centre, through the USGS/NEIC information feeds. This was 16 minutes after the event, but had an underestimated magnitude, causing a Green alert. The first Orange alert was based on information from NOAA, received 20 minutes after the event (again through the NEIC feeds). Later, the magnitude estimate was revised upwards and depth downwards, increasing the alert level to Red (with a grid-based tsunami wave height of 4.01m).

Table 6 - List of epicentres identified by the GDACS system, as they were collected¹⁷

Alert level	Estimated tsunami wave height (m)	Lat/Long	Magnitude (M)	Depth (km)	Source	Publication Date/Time (UTC)	Delay
	0.06	-15.27, -171.5	7.1	33	PTWC	9/29/2009 06:04:30 PM	16 min
	2.27	-15.4, -171.6	7.9	33	NOAA	9/29/2009 06:09:11 PM	20 min
	2.27	- 15.5538, -172.1409	7.9	35	NEIC	9/29/2009 06:14:51 PM	26 min
	2.27	-15.42, -172.21	7.9	60	EMSC	9/29/2009 06:14:59 PM	26 min
	2.27	-15.43, -172.2	8.1	60	EMSC	9/29/2009 06:30:02 PM	42 min
	4.01	-15.3, -171.0	8.3	33	NOAA	9/29/2009 07:05:59 PM	1h17min
	2.27	- 15.5577, -172.0726	8.0	18	NEIC	9/29/2009 07:37:36 PM	1h49min
	2.27	-15.3, -171.0	8.0	33	NOAA	9/29/2009 10:11:46 PM	3h23min
	3.3	-15.559, -172.0926	8.0	18	NEIC	9/30/2009 03:15:21 PM	>21h

While these response times are adequate for the international community, the systems would have been too slow to alert some of the most affected areas. The first tsunami waves arrived¹⁸ in Western Samoa 17 minutes after the earthquake. Most cities in Western and American Samoa were reached by the waves within 20 minutes. The highest waves (higher than 7 meters) and generated by local geographic conditions, arrived 30 minutes after the event.

Note that the uncertainty on the earthquake parameters caused an underestimation of wave heights: the maximum wave height reported by the GDACS system increased from 0.06m to 4.01m (1h17 minutes after the event), while the true maximum wave heights were in the order of 7m in American Samoa Islands and up to 20m in Tonga Islands. A detailed report on the automatic GDACS response can be found in (Annunziato, 2009).

4.1 The near-real time calculations

In this section only the final simulation (the last row in Table 6) is discussed. However, the results of all the other simulations are available online in the GDACS report pages.

The system was initialized with an initial maximum height of 3.16m. The maximum wave height near the coast indicated in the calculations is 3.8m in Fagamalo and Poloa and 3.1m in Fagasa, all in Tutuila Island (American Samoa Islands). This calculation, performed with 2.64 min grid size bathymetry (~ 4800 m) was not able to identify the small island where Niuatoputapu Village is located: however, a very high energy above that island is shown.

The comparison with the DART shows that the calculation anticipates the signal by 5 min and the height is overestimated (Figure 12 and Figure 13), while it is very close in height and period for the buoy signal in Pago Pago Bay, Tutuila Island (Figure 14). Nevertheless, the initial negative wave is not predicted because the early warning JRC fault model assumes an all-positive cosinusoidal shape in order to calculate a worst-case scenario.

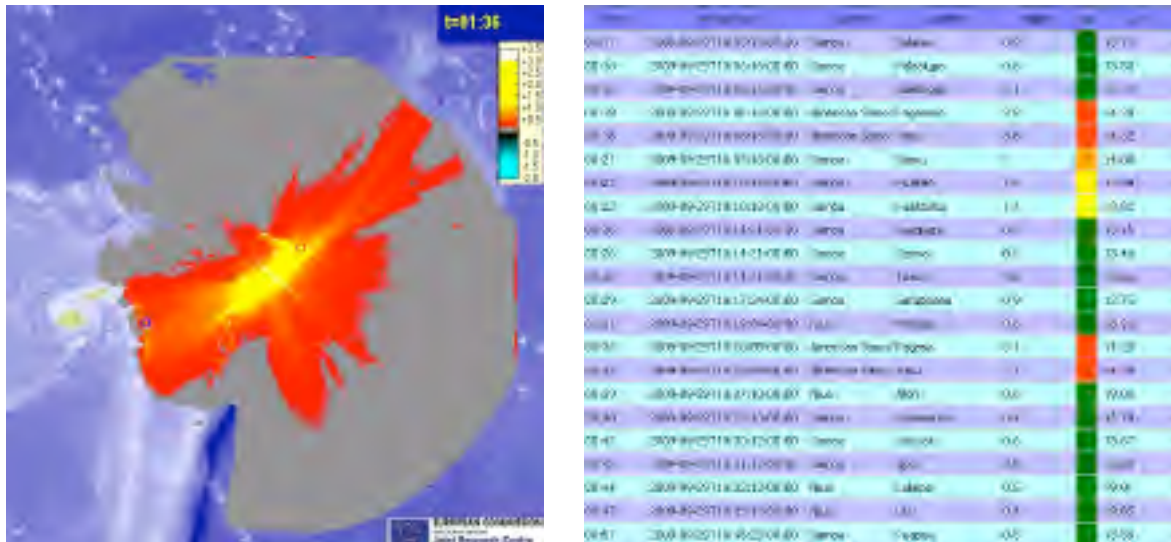


Figure 11 - Near-real time calculation of the Samoa event: on the left the maximum calculated height, on the right the list of identified locations and wave height

The early-identified localities are compared with UNOSAT damage assessment (see Figure 15 and Figure 16). Most of the assessed localities in Savai'i & Upolu Island are identified by the early warning system. In Tutuila Island some of the affected localities identified by the early warning are in the opposite side of the small Island, which is from 5 to 10 km in extent, i.e., on the same order of magnitude as the grid size. However, the objective of alerting the islands has been achieved.

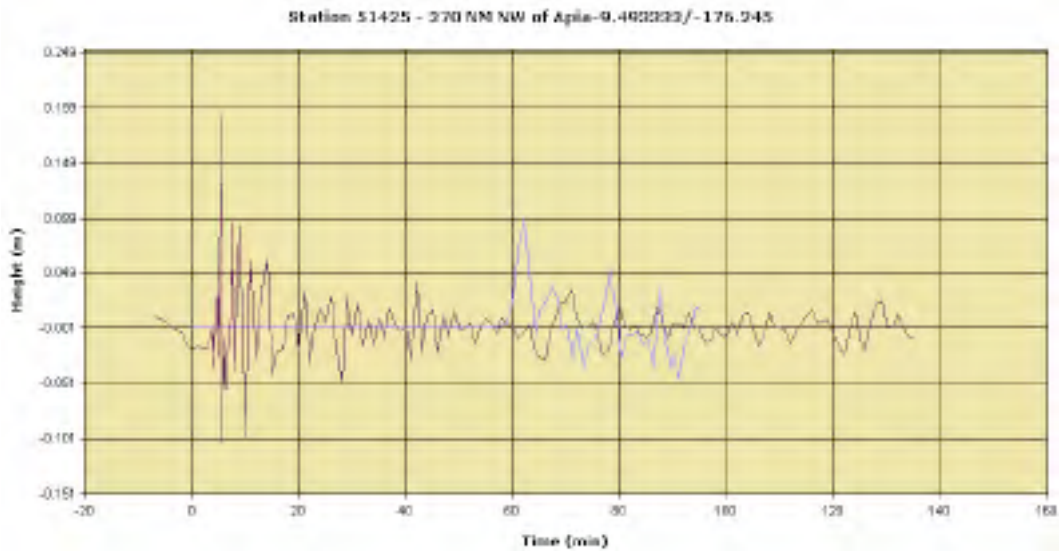


Figure 12 - Comparison of sea level indication from the 51425 DART buoy (red) with the near-real time calculation (blue). Note the oscillation from time 0 min to 60 min in the DART buoy, which are due to the seismic pressure wave transmission.

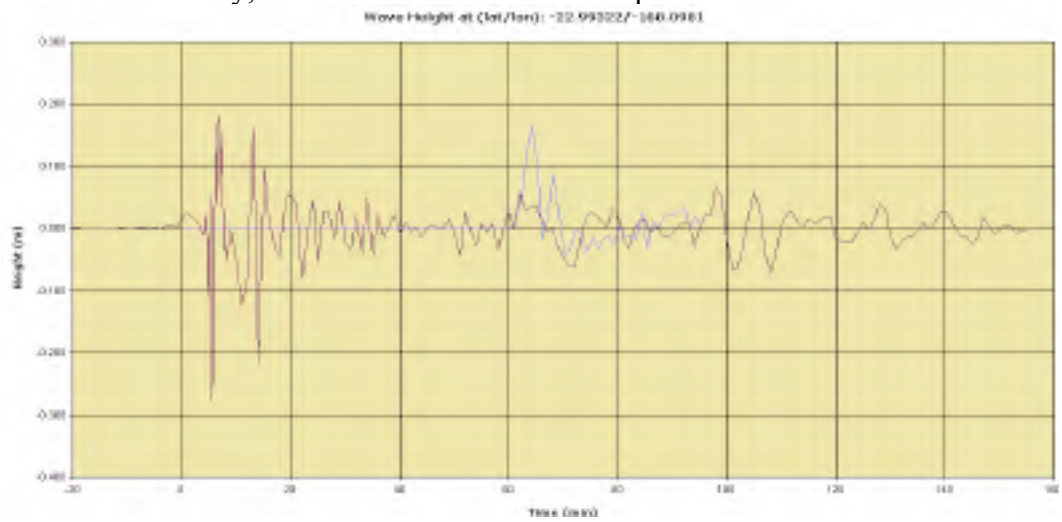


Figure 13 - Comparison of sea level indication from the 51426 DART buoy (red) with the near-real time calculation (blue)

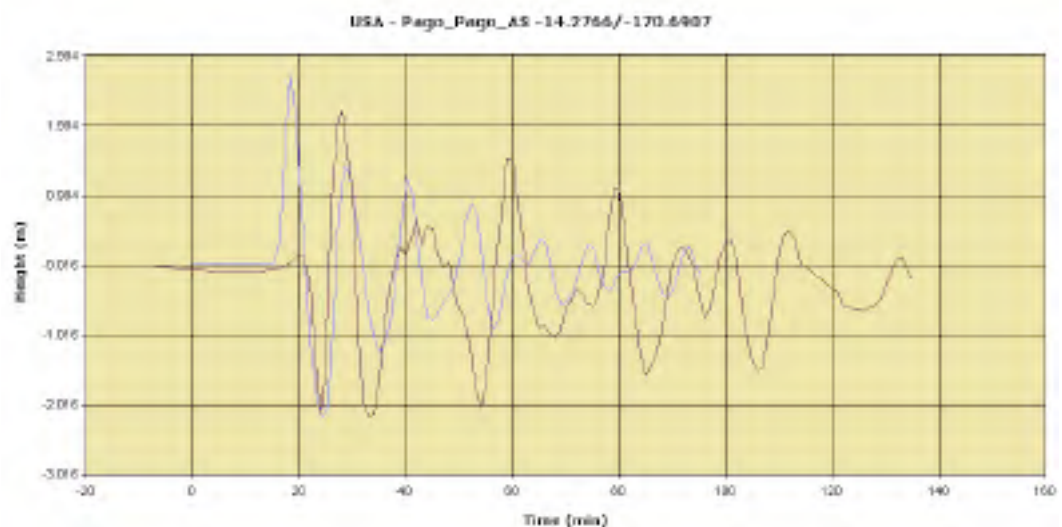


Figure 14 - Comparison of tidal level in Pago Pago (red) with the near-real time calculation (blue)



Figure 15 - Savai'i & Upolu Island. Comparisons of UNOSAT damage assessment and locations (see the place marks) identified by the JRC early-warning system.



Figure 16 - Tutuila Island. Comparisons of UNOSAT damage assessment map and locations (see the place marks) identified by the JRC early-warning system

4.2 Alert and Models Assessment

Alert assessment is performed in the hours immediately after the event. Together with the objective to assess the early warning launched by retrieval of pre-calculated grid scenario and near-real time simulations, the aim is also to quickly estimate the impact of the tsunami at a more detailed regional scale: in fact the grid size of the near real-time calculations are coarser (~ 4800m) in order to cover a wider window.

In the next section, first the fault sources using the SWAN JRC code are assessed and then the predictions provided by the codes available at the JRC, i.e., SWAN, HyFlux2 and TUNAMI-N2 are assessed.

4.2.1 Fault assessment

In this section are shown the comparisons of the simulations performed by the SWAN JRC code using different fault sources described in section 0 which are available after the event, i.e., USGS-CMT, Harvard CMT and Finite Fault Model. The run grid size is 1800 m.

The fault assessment is based on the available DART measurements (DART 51425 and 51426) and tidal buoy measurements (Pago Pago bay on Tutuila Island and Apia bay on Opolu Island) whose positions are shown in Figure 2.

In Figure and Figure , the comparisons of DART measurements with simulations performed using different fault models are shown. At a first glance, none of the simulations seems to provide good accuracy with the measurements: on both DART's the effects of the p-wave continue until the tsunami (gravitational) wave arrives, providing a measured positive wave on DART 51426, which is opposite with respect to the simulations.

The reason for this prolonged effect of the p-wave as well as its influence on the DART measurement is not well understood or quantified. Probably a best-filter algorithm could improve the quality of the signal. A first explanation could be that the tsunami wave propagates mainly northeast and southwest, while the DART measurements are northwest and southeast of the epicentre, with a consequent lower amplitude of the tsunami gravity wave in respect of the DART directions. Therefore more detailed studies on the use of the DART measurements are necessary.

However, comparing the arrival time and the amplitude of the first measured negative wave with the simulated ones, it can be stated that the Finite Fault Model provides the best wave simulations, while the Harvard CMT Fault model provides the worst ones.

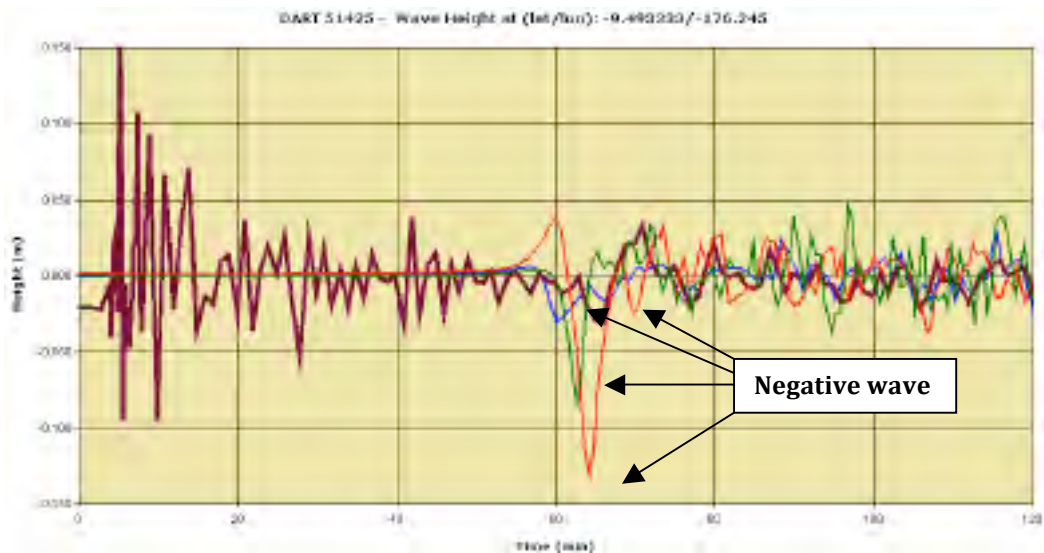


Figure 17 - Comparisons of DART 51425 level (brown) with simulations based on Harvard CMT (red), USGS CMT (blue) and Finite Fault Model (green)

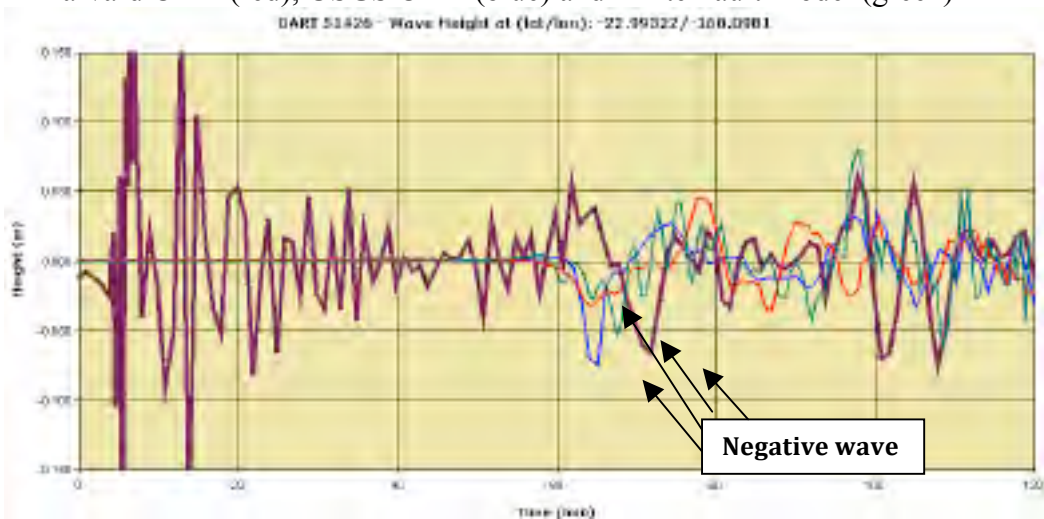


Figure 18 - Comparisons of DART 51426 level (brown) with simulations based on Harvard CMT (red), USGS CMT (blue) and Finite Fault Model (green)

In Figure 19 and Figure 20 the comparisons of buoy measurements with simulations performed using different fault models are shown. On both tidal buoys the first significant wave is negative as in the simulations. The arrival time of the simulations is anticipated in respect to the measurements. One can note that the tidal buoy measurements are not disturbed by the p-wave like on the DART, because a gravitational instrument is used. In Apia bay the simulated wave amplitude is on the same order as the measurements, while in Pago Pago bay they are halved.

The simulations show more oscillations when compared with measurements. Such behaviour can be explained by numerical problems that the finite difference models suffer when the wave approaches the coast.

Also for the buoys it can be stated that the Finite Fault Model provides the best wave simulations, while the Harvard CMT Fault model provides the worst ones.

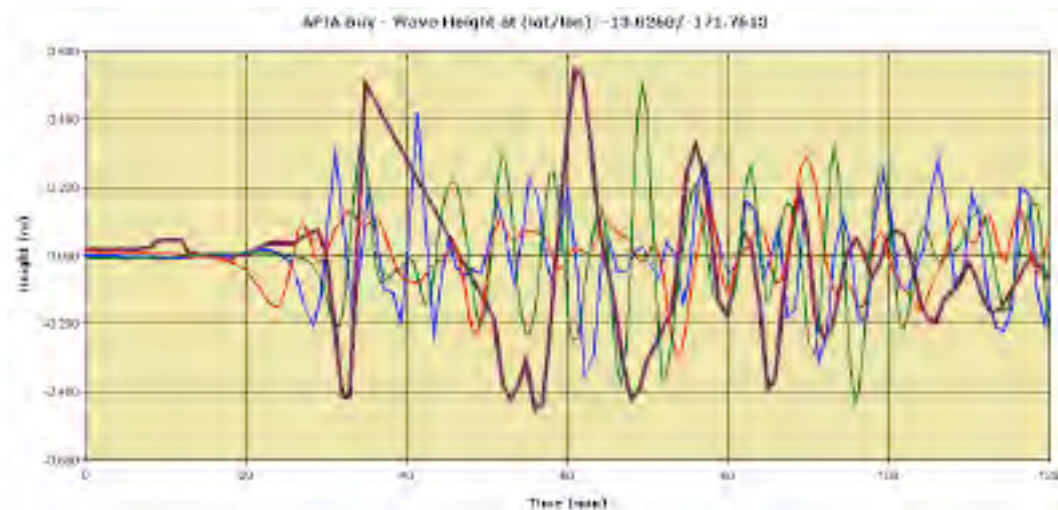


Figure 19 - Comparisons of Apia bay level (brown) with simulations based on Harvard CMT (red), USGS CMT (blue) and Finite Fault Model (green)

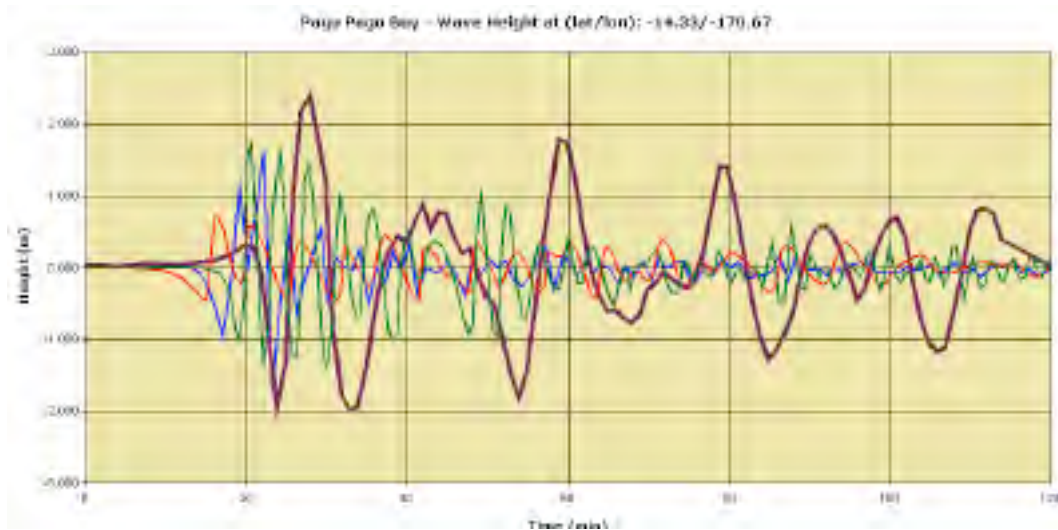


Figure 20 - Comparisons of Pago Pago bay level (brown) with simulations based on Harvard CMT (red), USGS CMT (blue) and Finite Fault Model (green)

4.2.2 Model assessment

In this section are shown the comparisons of the simulations performed by the SWAN JRC code, TUNAMI-N2 and HyFlux2, using as initial conditions the crust deformations provided by the Finite Fault Model. The grid size is 1800 m. In Figure 21 and Figure 22, the comparisons of DART measurements with simulations performed using different codes are shown. The first wave simulated by SWAN-JRC and HyFlux2 is exactly the same. TUNAMI-N2 shows small differences in respect to the previous ones. After the first wave, SWAN-JRC and TUNAMI-N2 show oscillations whose amplitude and frequency are not present in the measurement, and may be considered artefacts as a result of numerical instabilities. HyFlux2 simulations are smoother, with decreasing amplitude.

Similar behaviour can be noted in Figure 23 and Figure 24. The two Finite Difference codes, SWAN-JRC and TUNAMI-N2, continue to show oscillations which

are more evident in the second one, while the Finite Volume code, HyFlux2, is still smoother, but with waves that show lower amplitude in respect to the measurements and the results from the other codes.

The tendency in HyFlux2 code to provide smooth simulations (without numerical oscillations) is a desirable property because in such cases, when oscillations are predicted, they can be imputed to physical reasons and not to numerical artefacts. On the other hand, the results of HyFlux2 are damped: such behaviour disappears when the grid size resolution is higher, providing consistency with the geometry of the coastline. Simulations with higher resolution will be shown in the next section.

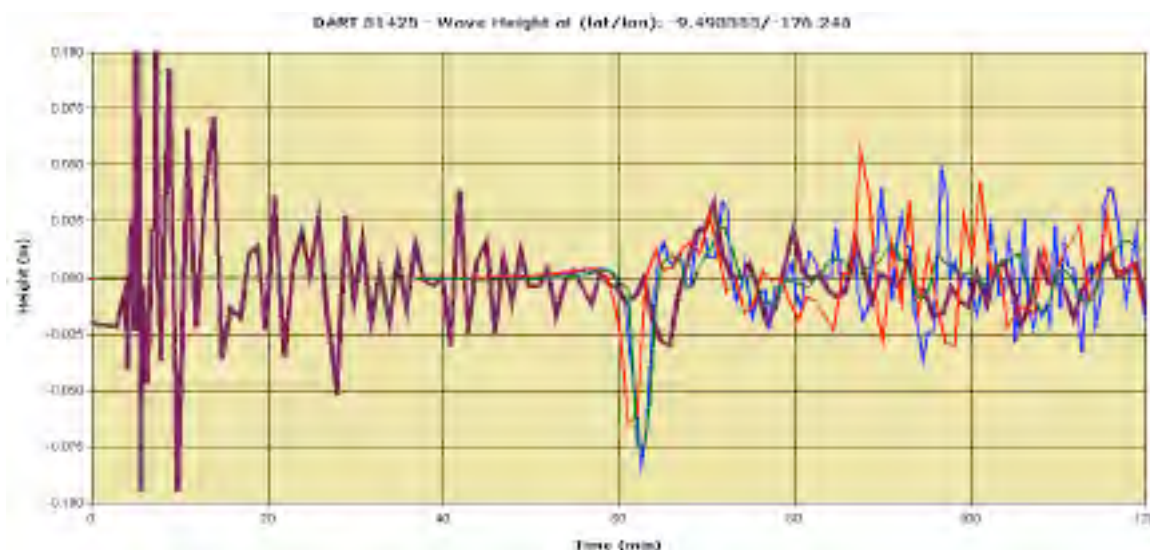


Figure 21 - Comparisons of DART 51425 level (brown) with simulations based on TUNAMI-N2 (red), SWAN JRC (blue) and HyFlux2 (green)

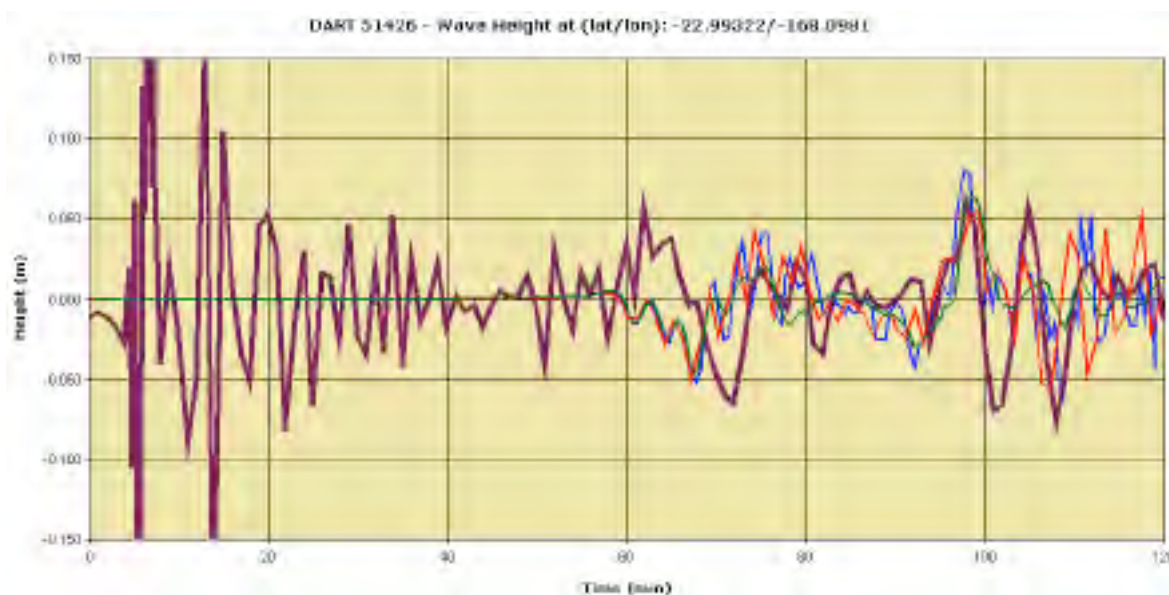


Figure 22 - Comparisons of DART 51426 level (brown) with simulations based on TUNAMI-N2 (red), SWAN JRC (blue) and HyFlux2 (green)

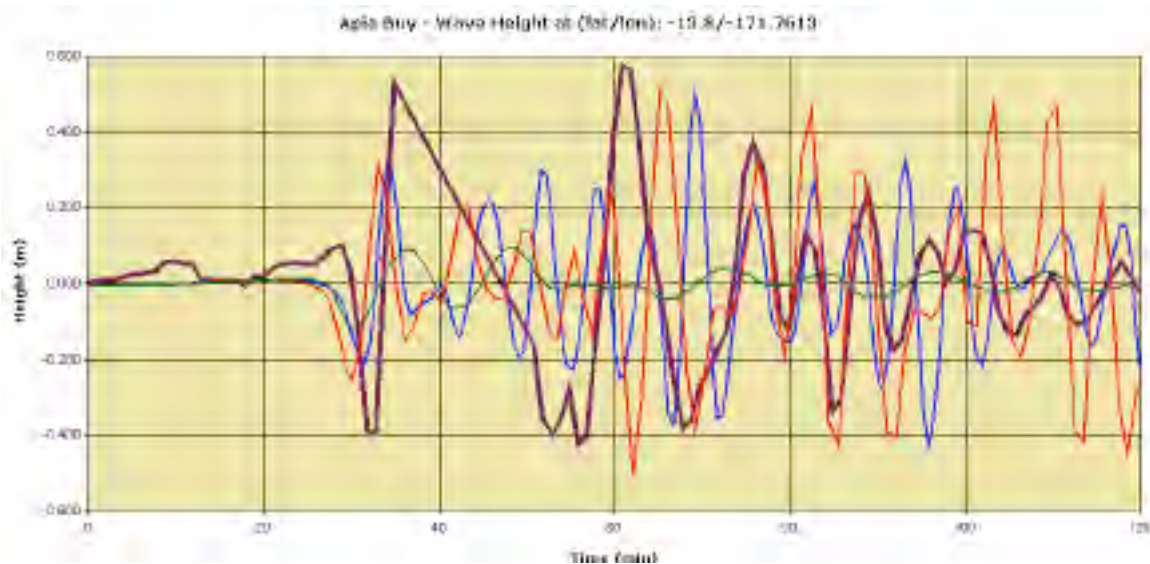


Figure 23 - Comparisons of Apia Bay level (brown) with simulations based on TUNAMI-N2 (red), SWAN JRC (blue) and HyFlux2 (green)

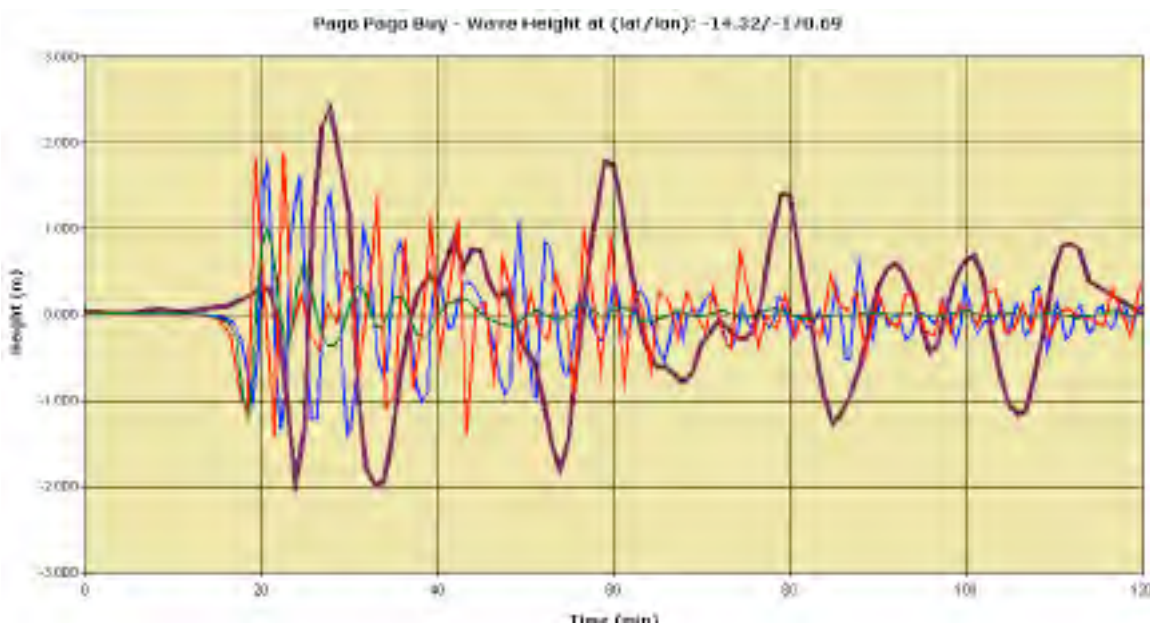


Figure 24 - Comparisons of Pago Pago Bay level (brown) with simulations based on TUNAMI-N2 (red), SWAN JRC (blue) and HyFlux2 (green)

5. INUNDATION MAPPING

The typology of the post event calculations depend on the objectives of the simulations and on the available DEM:

- *Early run-up area identification.* The objective here is to identify more precisely the affected locations and try to estimate the water level at the shoreline and the potential inundation in the various coastal areas. The requested grid size is on the order of 100 to 300m.
- *Inundation assessment.* The objective is to precisely identify the inundated area and run-up and evaluate the impact on buildings and infrastructure. The requested grid size is on the order of 10 to 30m.

The worldwide available DEM has a cell grid size of 30 arc sec (see Table 5), which corresponds to about 900m, so the best detailed simulation that can be done using such a source grid size cannot be significantly smaller. For the Samoa 2009 tsunami event, detailed DEM are also available for the American Samoa Island: this is an ideal opportunity to analyse which source grid size is the most suitable for the different simulation typologies and which are the most detailed simulations that can be done with the worldwide available 900m DEM grid size. In Table 7 are shown the performed runs.

Table 7 - Calculation grid size Vs source grid size. Calculation with grid size from 300m to 10m is nested from the coarser ones. The arrows indicate the flow of information for the nested simulations.

		Source Grid Size		
		900	90	10
Run Grid Size	1800	x		
	900	x ↓		
	300	x ↓	x ↓	
	90	x	x ↓	
	30		x	x ↓
	10			x

Simulations with run grid size of 300m and less are done using the results of the coarser one as boundary conditions. The window is reduced in order to maintain the total number of cells on the order of 1 million. Such nested computational grids – from coarse the high-resolution – are used to have a minimum number of nodes spanning a wavelength in order to resolve the wave with finer detail, considering also that the wave length decreases when approaching the coast.

The reason for performing more detailed calculations in subsequent steps, with smaller window and cell size, is that the required CPU time increases as a cubic function of the cell size reduction, i.e., if the cell size is halved and the window remains the same, the number of cells becomes 4 times higher and the CPU time becomes 8 times higher. On the other hand, detailed information is useful only near the coast and not in the open sea where the wavelength is so long that coarse simulations represent well the real behaviour.

5.1 Early run-up area identification

The aim of this section is to describe how the geographical areas that could be affected by tsunami run-up are identified. When the wave reaches shallow water, its wavelength becomes shorter and the surface level rises, due to the conservation of energy. Such phenomena are emphasized in bay areas, where reflection and resonance

take place. Therefore it is necessary to adopt very detailed cells to be able to specify the bathymetry, the shoreline and the possible run-up topography. The precision of such information will strongly influence the simulation accuracy, and the capability of the code to reproduce the real phenomena.

Unfortunately the best resolution of the worldwide available data on bathymetry and topography is 30-arc sec (~ 900 m). To interpolate the available DEM to very low grid size (i.e. smaller than 100 m) does not make sense, considering that the elevation of hills and bays of size smaller than 1 km are averaged to one grid cell in an elevation model of 1km grid size. Therefore the compromise for a quick identification of the inundated area is to make simulations with 300 m grid size bathymetry, which is interpolated from the 900 m available information. With such resolution the wavelength at the shore is quite well represented, but the information on run-up distance is quite poor when the measured values are lower than 300m or when simulating waves entering into bays whose width or length is on the order of 1 km.

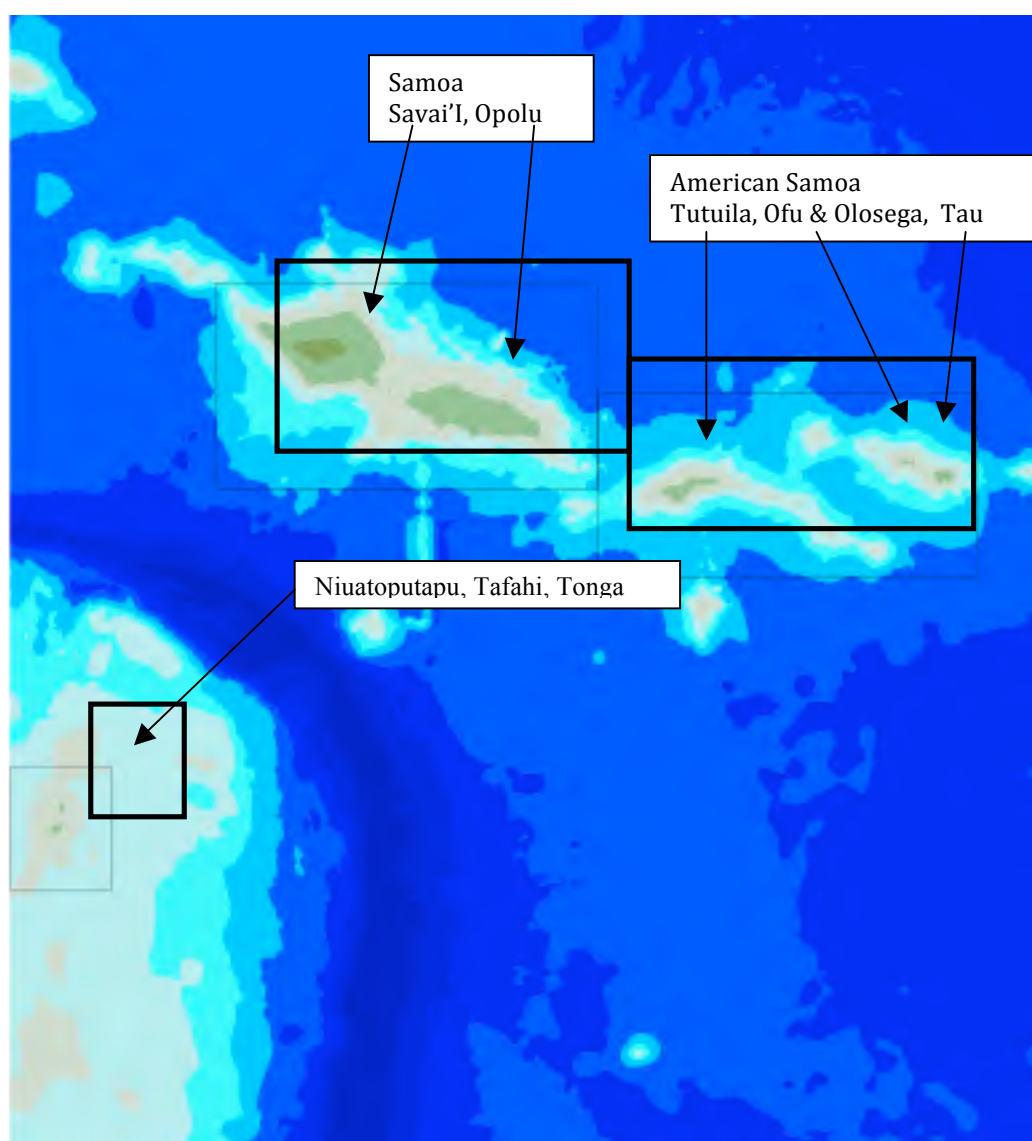


Figure 25 - Windows of the 300 m grid size nested simulations for early run-up identification.

Three nested simulations have been performed as indicated in Figure 25: the simulation result at 900 m grid size resolution (the larger window) is used as the boundary condition for the simulations with 300 m grid size (smaller windows). The crust deformation is provided by the Finite Fault Model.

HyFlux2 code has been used for inundation simulations. At identified (populated) locations, some estimation on the tsunami wave is provided. In Figure a sketch of the defined quantities is presented. All the quantities are evaluated within a 5 km radius from the point on the shoreline, which is the closest to the location of interest. Such a search radius decreases in case the simulation grid size resolution is very low and the number of localities in the search radius is high.

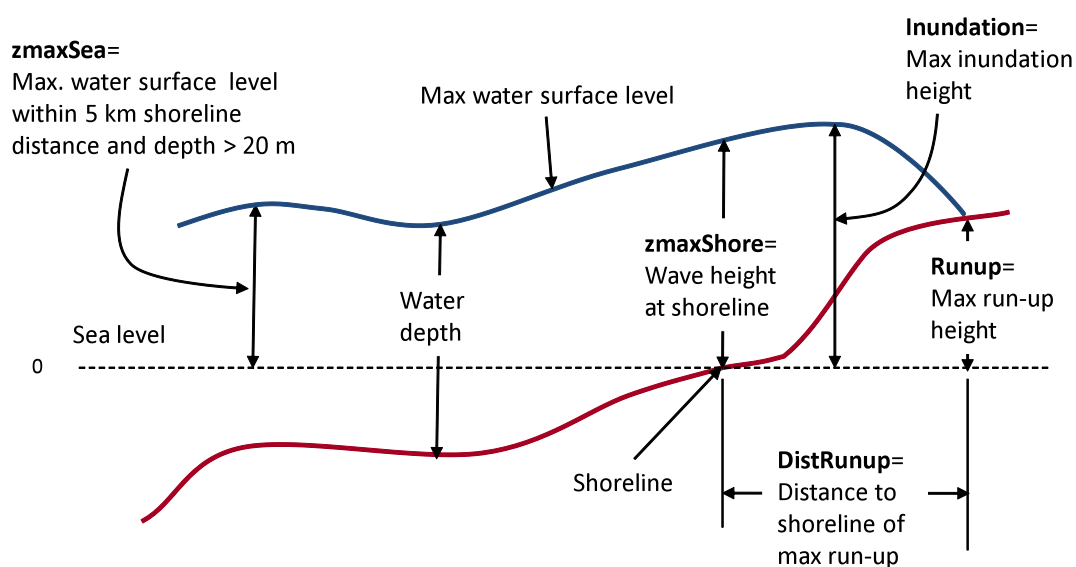


Figure 26 – Definitions on tsunami inundation quantities at selected evaluatee locations.

5.1.1 Saval'I and Opolu Island, Samoa

The Samoa Islands have been the most affected islands in the archipelago with more than 150 fatalities. The run-up areas and locations – identified by the simulation – are compared with the UNOSAT damage assessment image (Figure 27).



Figure 27 – Savai'i Island. Overlay of UNOSAT damage assessment map with the inundation map (landWet.map, distance from the shoreline [m]) and identified locations (push pin place marks).

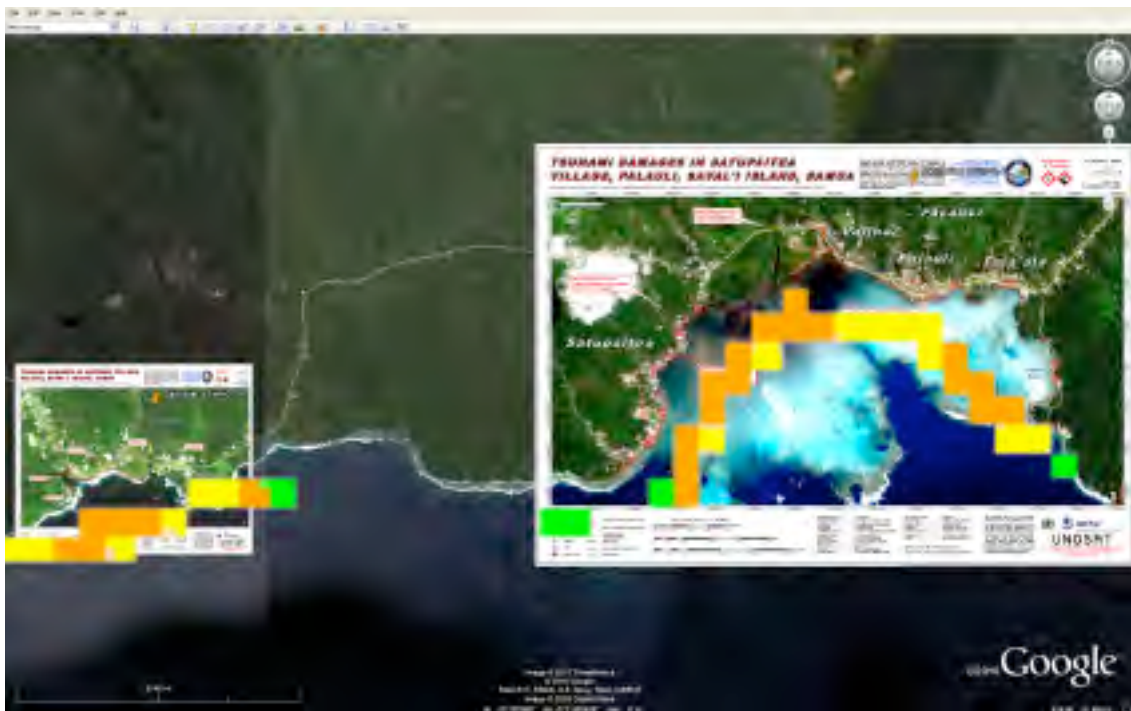


Figure 28 - Savai'i Island, Gautavi, Palauli, Satupaitea Villages. Overlay of UNOSAT damage assessment with the inundation map (landWet.map, distance from the shoreline [m]) and identified locations (place marks)

Most of the localities assessed by UNOSAT images are also identified by the simulations. In Saval'I Island Satupaitea locality, a maximum water height of 2.13 m has been simulated. In Figure 28 is a detail for some villages assessed by UNOSAT. It can be seen that, despite the rather coarse resolution (300m grid size) the simulation is able to identify the run-up areas like using images.



Figure 29 - Opolu Island. Overlay of UNOSAT damage assessment with the inundation map (landWet.map, distance from the shoreline [m]) and identified locations (push pin place marks)

On Opolu Island, Falease'ela locality, the maximum water height (simulated) reached 5.48 m. In addition, the simulations identify some localities in West and East side of Opolu Island that are not assessed by UNOSAT (Figure 8). In the Apia tidal buoy a maximum of 0.7m was measured (see Figure). Despite the fact that the buoy is downstream of the island, the simulated waves (amplitude, oscillation period and trend of decay) fit quite well with the available measurements.

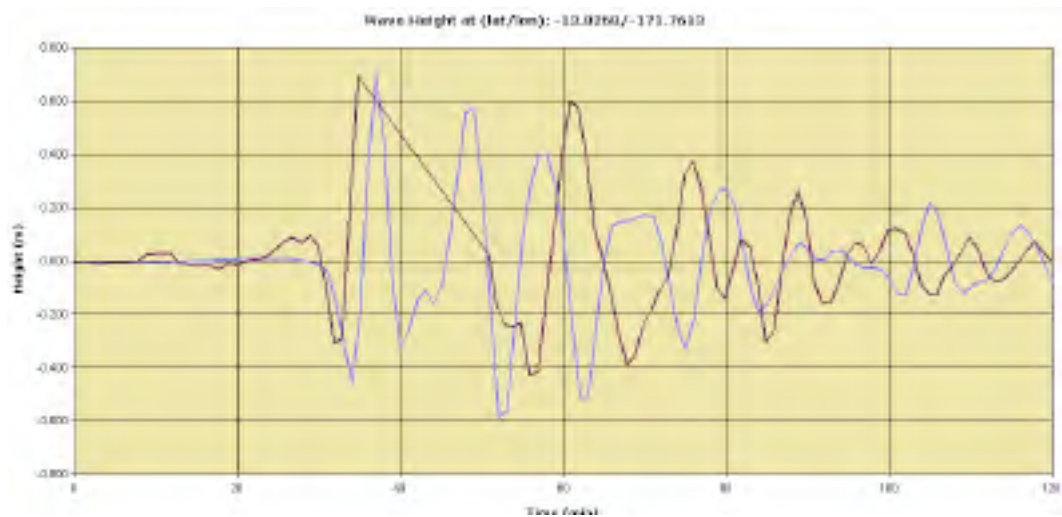


Figure 30 - Measured (red) and simulated (blue) water level at Apia bay. Measures from t=34 min and t=51 min are missing

5.1.2 Tutuila, Ofu & Olosenga, Tau, American Samoa

Tutuila Island was overcome by tsunami waves on the order of 5 to 7 m, with a splash height of 16 m in Poloa. There were 34 fatalities (see Table 1). The run-up areas and locations – identified by the simulation - are compared with UNOSAT damage assessment image (see Figure 31). In contrast to the Samoa Islands, where destruction was confined to the southern part, in Tutuila Island a significant impact has been measured (and simulated) on both the south and north coastlines. Note that the damage assessment based on satellite imaging has been performed only on the west part of the island because of cloud cover whereas the simulation and the post tsunami survey show inundations along the entire island coastline.



Figure 4 - Tutuila Island. Overlay of UNOSAT damage assessment with the inundation map (landWet.map, distance from the shoreline [m]), identified locations (push pin place marks) and post-tsunami survey (star place mark)

The negative wave reached Pago Pago Bay about 20 minutes after the initiating event, followed by a subsequent positive wave 5 minutes later. A comparison of the simulation results with the tidal buoy measurement is shown in Figure 32. The first wave is simulated quite well, but the frequency of the subsequent waves is different from those measured. These differences could be explained by the poor horizontal accuracy of the DEM, which makes the simulated bay shorter than the real one, with resulting differences between the simulated and measured wave period.

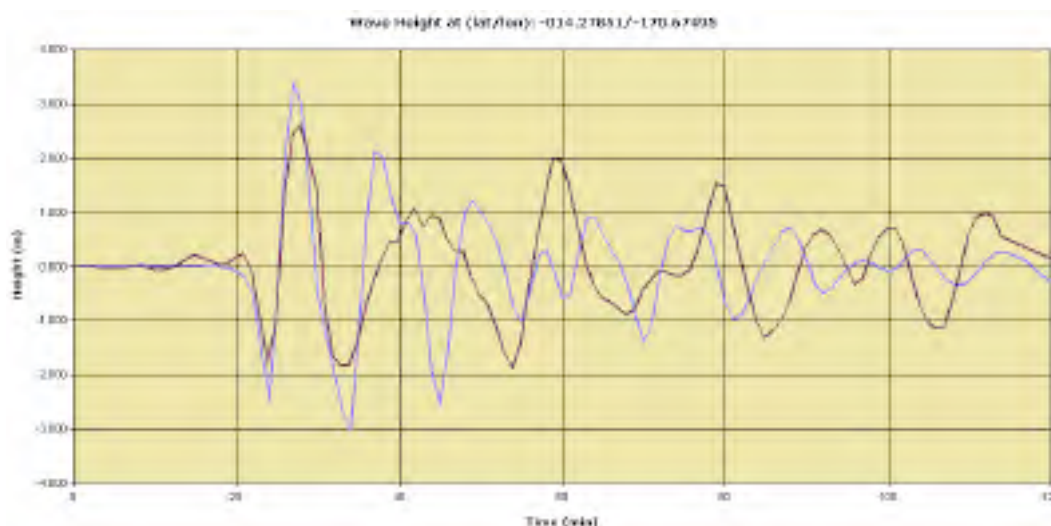


Figure 32 - Measured (red) water level at Pago Pago bay compared with simulated water height in a point out of the shoreline (blue)

Ofu, Olosega and Tau islands (east of Tutuila Island) were the islands with the highest simulated water run-up (see Figure 33). A maximum water level of 11 m was simulated in Ofu and 7 m in Olosega (measured 6.1m and 4m respectively). At Tau a maximum water level of about 5 m was simulated, while the measured level was 12 m.

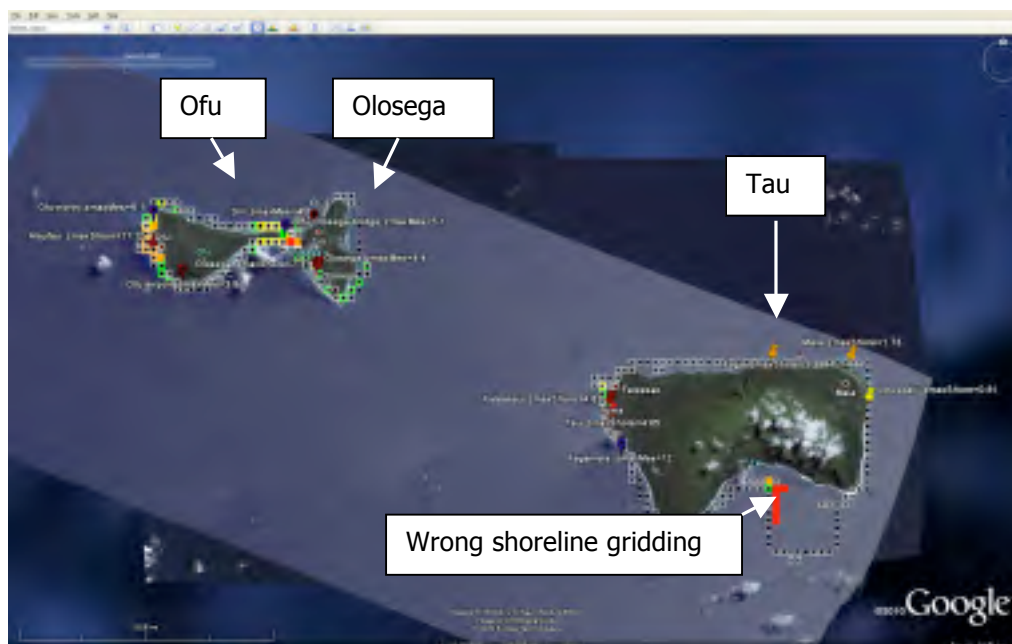


Figure 33 - Ofu, Olosega, Tau Isl. Inundation map and identified locations.

In Figure 34, a comparison of measure data and code simulations is shown. The numerical model under predicted the measurements in Tutuila, over predicted in Ofu & Olosega Islands, and under predicted again in Tau Island. The average of the ratio between prediction and measurement is 0.73 in Tutuila and Tau Island, while it is about 1.66 in Ofu & Olosega. Such differences, as discussed above, can be explained by the coarse and sometimes inappropriate shoreline gridding.

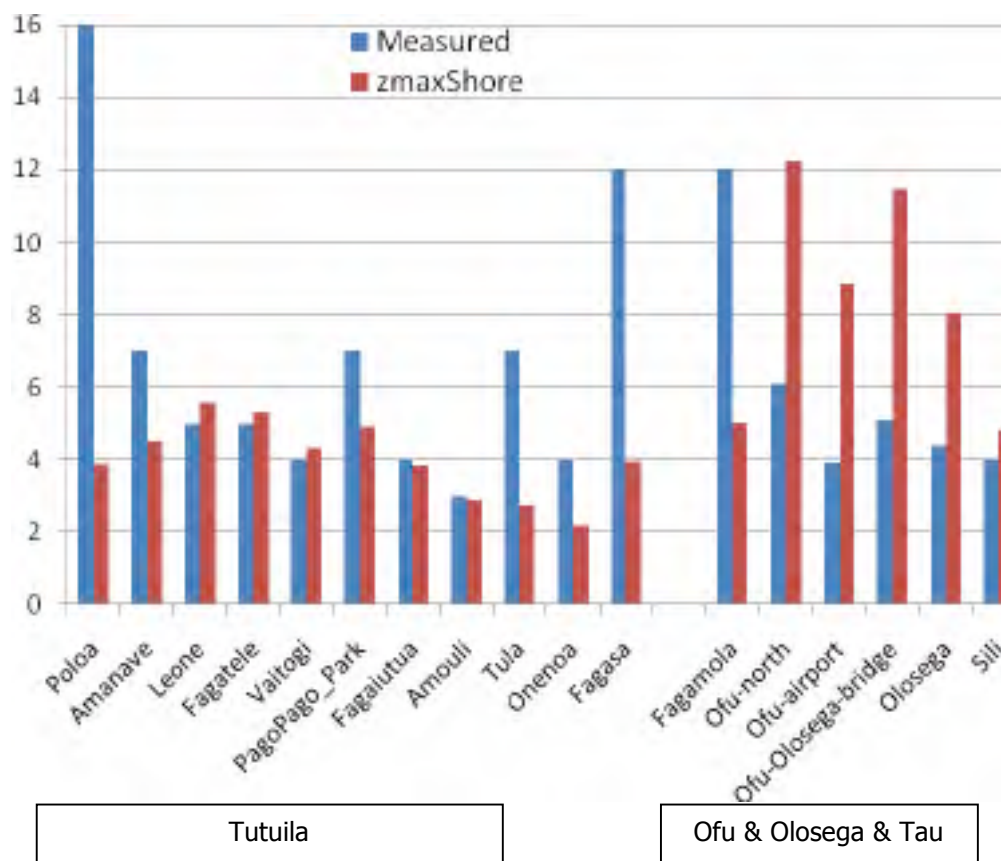


Figure 34 - Comparisons of measured run-up with the simulated water surface level at the shoreline (zmaxShore).

5.1.3 Niuatoputapu & Tafahi, Tonga

The tsunami impact on these islands was very high. A maximum run-up (EERI, 2010) of 22 m was measured at Tafahi Island and 15 m at Niuatoputapu Island, while maximum water surface level of about 7 m was simulated at both the islands. Major impacts have been surveyed along the east coast. The extended coral reef reduced the impact on villages on the west and north sides of the coastlines. In Figure 35 is shown the inundation map, which is qualitatively confirmed by the observations.

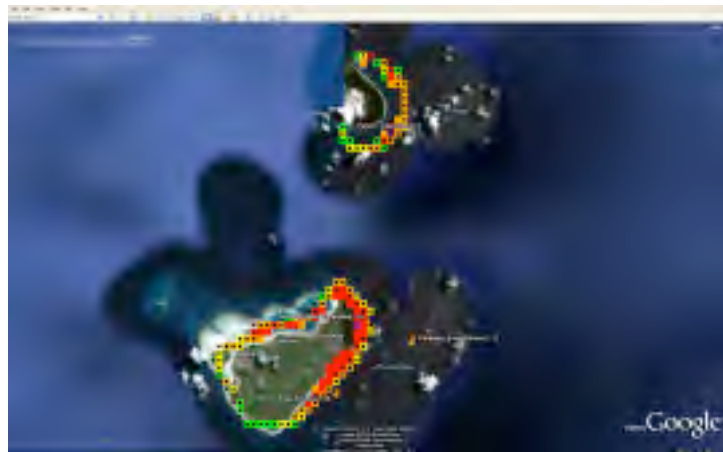


Figure 35 - Niuatoputapu, Tafahi Island. Inundation map and identified locations.

6 INUNDATION ASSESSMENT

The objective of an inundation assessment is to quantify the inundation extent in identified run-up areas. For this purpose, the use of high-resolution grids is necessary not only in ensuring accuracy and reliability of the simulations but is essential when describing local details like narrow bays, estuaries, harbours or in general any run-up areas affected by inundation.

In Figure 36, simulations with 300 and 90 m grid size respectively are shown. On both maps, the inundated localities are identified but, due to the coarse accuracy of the source data, the coastline is smoothed and the quantification of the inundation area obtained by the finer 90m simulation is not reliable. Increasing the simulation accuracy is not enough when the objective is to identify the extent of the inundated area. Therefore DEM data with higher accuracy is necessary for better inundation assessment.

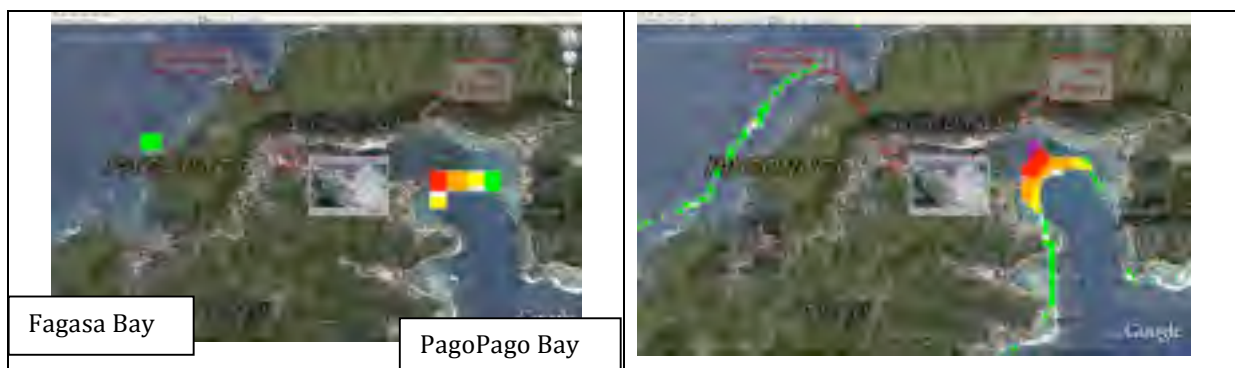


Figure 36 - Pago Pago and Fagasa bays. Inundation maps for simulations with grid size 300m (left) and 90m (right) interpolated from 900m grid (STRM30+)

For the Samoa 2009 Tsunami event, detailed DEM - 3 arc-second and 1/3 arc-second data, which correspond to about 90m and 10m - are available for the American Samoa Islands (see Table 5 and E.Lim, 2010). This very rare DEM availability provides an ideal opportunity to assess the HyFlux2 capabilities on inundation simulation. Another important issue is to analyse which grid-size simulation is the most suitable for inundation assessment: this is not a trivial exercise considering that the computer resources needed (CPU time and memory) drastically increase with increasing accuracy of the simulations.

Nested simulations with 90m, 30m and 10m-grid size accuracy have been performed. In Figure 37 are presented the inundation maps produced by 90 m (left) and 30 m (right) grid size simulations. In both simulations the DEM has been interpolated from a 90m grid. Contrary to the simulation performed at the same grid size (90 m) but interpolated from 900m, now the shoreline is captured more correctly, providing hot spots much more consistent with the observations. With 30m-grid size simulation the run-up line and inundation extent is captured with more detail.

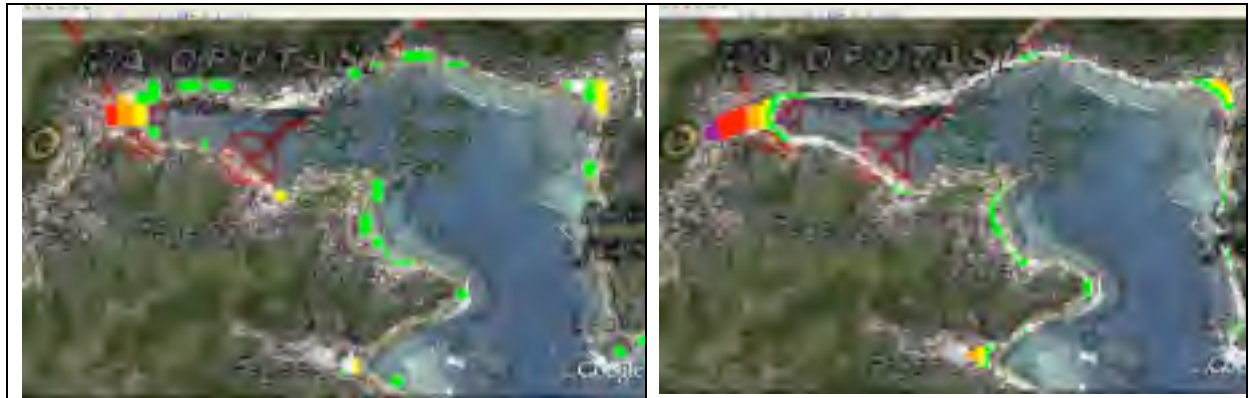


Figure 37 - Pago Pago bay. Inundation maps for simulations with grid size 90m (left) and 30m (right) interpolated from 90m grid (NOAA - AS 3 arc-second Pago Pago, see Table 5)

In Figure 38, inundation maps are presented produced by 30m (top) and 10m (bottom) grid size simulations, using a DEM interpolated from a 10m-grid size. The extra effort in CPU time (factor of 27) and memory (factor of 9) spent in producing the 10m simulation is not compensated by the negligible increase in accuracy of the results.





Figure 38 - Pago Pago Bay. Detailed inundation maps for simulations with grid size 30m (top) and 10m (bottom) interpolated from 10m grid. (NOAA - AS 1/3 arc-second Pago Pago, see Table 5)

In Figure 39, the inundation maps at 30m-grid size resolution are shown, with the DEM interpolated from 90m and 10m-grid size respectively. Only in the airport region did the inundation maps show a different degree of detail. In general, a 30m-grid size simulation is sufficient when an inundation assessment is required. A 10m (or smaller) grid size simulation could be of interest in case an impact assessment on buildings and local infrastructure is required.

The numerically simulated inundation maps performed at 30m grid size resolution are at least as accurate as the satellite image maps; however, with the simulations, additional locations not assessed by satellite images have been identified. It is worthwhile to note that the damage assessment performed through satellite imaging was significantly restricted by heavy clouds and shadow, so the southern and eastern coasts in Tutuila Island were not assessed.

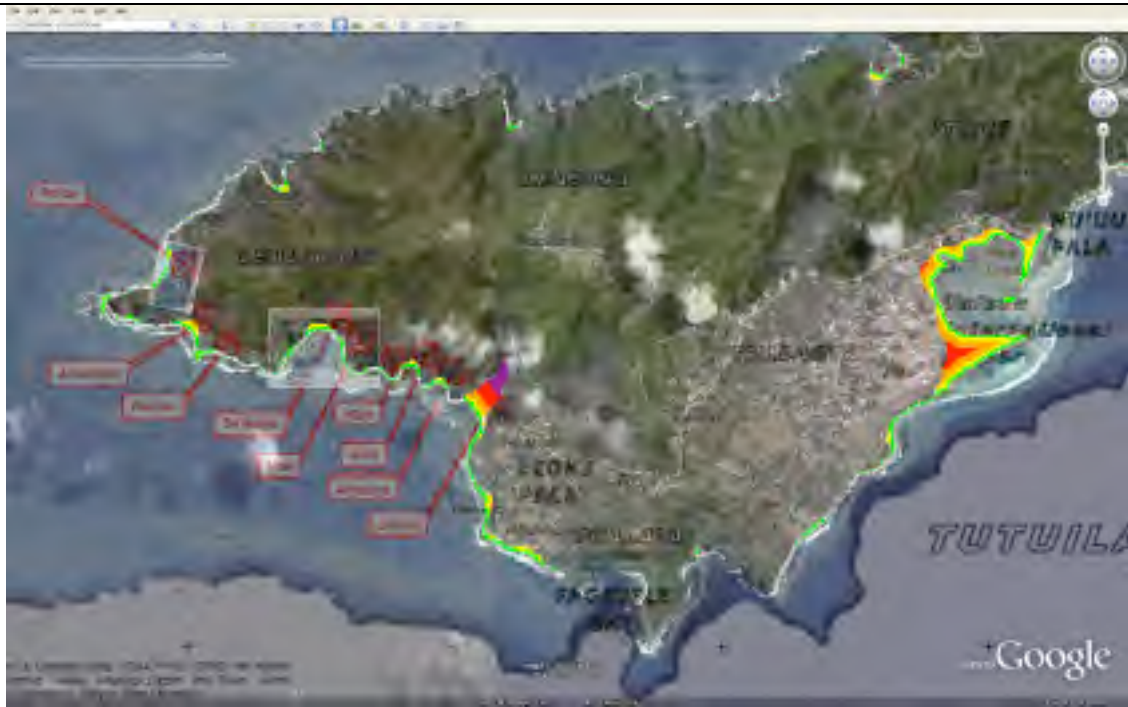


Figure 39 - East of Tutuila Isl. - Inundation maps for simulations with 30m grid size, interpolated from 90m grid (top) and 10m grid (bottom)

In Figure 40, a comparison of the post-tsunami survey measurements and simulation results are shown. The following observations can be drawn:

- Increasing the simulation accuracy, the simulated average $z_{maxShore}$ increases,

from 1.1 m (1800 m run grid size) to 6 m (30 m run grid size). With the same simulation accuracy (but different data sources grid size), the simulated averages are more or less the same, but with different values considering the localities individually. This is particularly true for the 300 m and 90 m grid size runs.

- The average maximum height at the shore of 3~4 m has been calculated by a 300m run grid size: the same values in open sea were calculated also by the near-real time calculations performed at 4800 m grid size, but with a conservative fault (see section 4.1).
- The standard deviation (*stdev* in Figure 40) of the measurements (about 4 m) is rather high when comparing with the average value (6.8 m). This could indicate that, sometimes, values that are not representative of the area are included into the observations, such as local “splashes” due to 2D steep gradients in the DEM, i.e., the measurements in Poloa (16.3m) and Fagasa (12m) could correspond to such cases.
- The standard deviation of the simulations continues to increase with increasing simulation accuracy, from 0.4m (1800m run grid size) to about 2m (10m run grid size). To reach the standard deviation of the measurements should require a very high accuracy, at least on the order of several meters, including in the bathymetry/topography the influence of buildings, roads and other infrastructures.

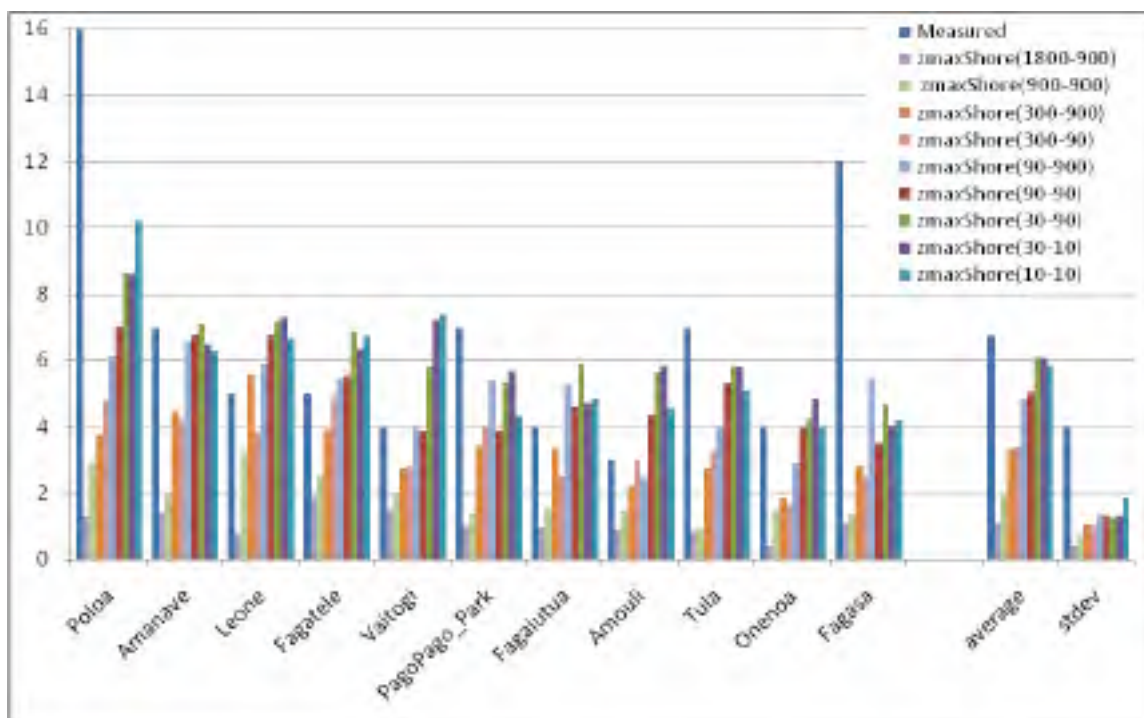


Figure 40 - Tutuila Island. Comparisons of measured run-up with the simulated water surface level at the shoreline. The labels zmaxShore (x-y) indicate simulations performed at x grid size, with DEM interpolated from y data source grid size

In Figure 41 are compared the inundation quantities evaluated at the localities where a maximum water height has been measured. In all these localities the trend is similar, indicating that the code is able to capture the physical run-up process. The average ratio between maximum inundation level and maximum surface level on the sea is about 1.46 ± 0.3 .

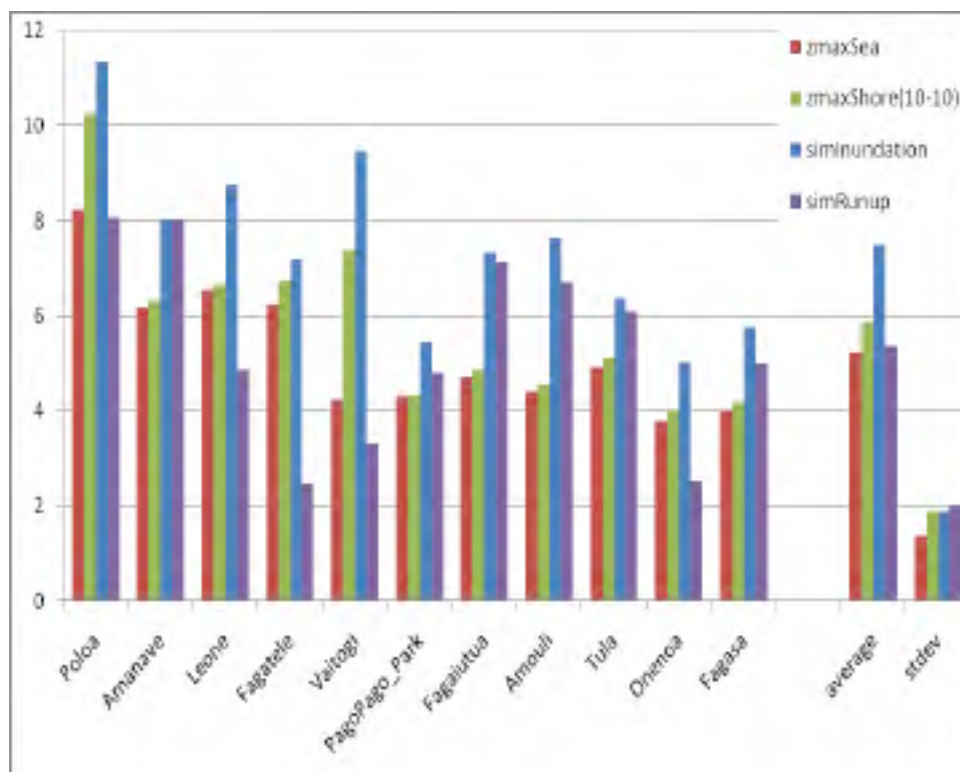


Figure 41 - Tutuila Island. Comparisons of tsunami inundation quantities (see also Figure 26 for definitions) evaluated by a 10 m run grid size

7 CONCLUSIONS

This report highlights the characteristics and impact of the tsunami that occurred in Samoa on 29 September 2009, describing the event, the available measurements in the months after the event and the seismological situation of the area.

It was shown that the GDACS system was able to give a correct preliminary estimate of the scale of the event, indicating which islands were likely to be affected by tsunami run-up.

An assessment of the simulation results of the SWAN-JRC code (used by GDACS) obtained from the initial conditions calculated by different fault models indicates that the Finite Fault Model best represents the event. The assessment also considers several hydrodynamic models, indicating that the wave propagation is modelled with the same level of accuracy by the SWAN-JRC, TUNAMI and HyFlux2 codes, despite the fact that the first two codes use a finite difference modelling approach while the third, developed particularly for inundation modelling, is a finite volume model. Differences between the codes have been seen when the wave approaches the coastline, showing oscillations in the results of the finite difference codes.

In order to draw up a more detailed map of the situation, finer calculations were performed after the event using the HyFlux2 code, identifying the most severely affected areas. It was concluded that a 300 m run grid size is adequate for early identification of the run-up area.

It was also attempted to evaluate the extent of inundation using a detailed digital elevation model, available for the American Samoa. The flooded areas for which we had satellite images and a post tsunami survey were in effect flooded and the extent of the maximum water surface level was estimated with a good accuracy.

It was concluded that a 30m run grid size is enough to estimate the flooding extent. Additional flooded areas not assessed by the satellite images - because of heavy clouds and shadow when the images were acquired - have been identified by the hydrodynamic simulations.

8. ACKNOWLEDGMENTS

The authors wish to thank Brian Worth for the careful reading and editing of the manuscript.

9 BIBLIOGRAPHY

Annunziato A. The Tsunami Assessment Modelling System by the Joint Research Centre [Article] // Science of Tsunami Hazards. - 2007. - Vol. 26(2).

Annunziato A., Franchello, G., Ulutas, E., De Groeve, T. 29 September 2009 Samoa Tsunami [Report] : JRC Scientific and Technical Reports. - [s.l.] : European Communities, 2009. - EUR Report 24068 EN.

Audusse E. [et al.] A fast and stable well-balanced scheme with hydrostatic reconstruction for shallow water equations [Journal]. - [s.l.] : SIAM J.Sci.Comp., 2004. - Vol. 25 (6). - pp. 2050-2065.

Beaven J. [et al.] Near-simultaneous great earthquakes at Tongan megathrust and outer rise in September 2009 [Journal]. - [s.l.] : Nature, 2010. - doi:10.1038/nature09292.

Brufau P. and Garcia-Navarro P. Unsteady free surface flow simulation over complex topography with a multidimensional upwind technique [Journal]. - [s.l.] : Journal of Computational Physics, 2003. - 2 : Vol. 186. - pp. 503-526.

Cruz A., Krausmann E. and Franchello G. Analysis of tsunami impact scenarios at an oil refinery [Article] // Natural Hazards. - [s.l.] : Springer Netherlands, 2010. - 10.1007/s11069-010-9655-x.

EERI Samoa Earthquake and Tsunami of September 29, 2009 [Online] // EERI Earthquake Engineering Research Institute. - January 2010. - September 22, 2010.

Franchello G. and Krausmann E. HyFlux2: a numerical model for the impact assessment of severe inundation scenario to chemical facilities and downstream environment [Report] : JRC Scientific and Technical Reports. - 2008. - EUR 233354 EN, ISSN 1018-5593E.

Franchello G. Modelling shallow water flows by a High Resolution Riemann Solver [Report] : JRC Scientific and Technical Reports. - 2008. - EUR 23307 EN.

Franchello G. Shoreline tracking and implicit source terms for a well balanced inundation model [Article] // Int. Journal for Numerical Methods in Fluids. - [s.l.] : Wiley, 2010. - Vol. 63. - pp. 1123-1146. - <http://www3.interscience.wiley.com/journal/122528271/abstract>.

Imamura F., Yalciner C. and Ozyurt G. Tsunami Modelling Manual (TUNAMI model) [Online] // DCRC -Tsunami Engineering Laboratory, TOHOKU University. - 2006. –

<http://www.tsunami.civil.tohoku.ac.jp/hokusai3/J/projects/manual-ver-3.1.pdf>.

Ji C., Wald D. J. and Helmberger D. V. Source description of the 1999 Hector Mine, California, earthquake, part I: Wavelet domain inversion theory and resolution analysis [Article] // Bull. Seismol. Soc. Am.. - 2002. - Vol. 92. - pp. 1192-1207.

Lay T. [et al.] The 2009 Samoa-Tonga great earthquake triggered doublet [Journal]. - [s.l.] : Nature, 2010. - doi:10.1038/nature09214.

Liang Q. A structured but non-uniform Cartesian grid-based model for the shallow water equations [Journal]. - [s.l.] : Int. J. Numer. Meth. Fluids, 2010. - DOI: 10.1002/flid.2266.

Liang Q. Flood simulation using a well balanced shallow flow model [Journal]. - [s.l.] : Journal of Hydraulic Engineering, 2010. - 669 : Vol. 136. - doi:10.1061/(ASCE)HY.1943-7900.0000219 .

Liang Q. Simulation of dam- and dyke-break hydrodynamics on dynamically adaptive quadtree grids [Journal]. - [s.l.] : Int. J. Numer. Meth. Fluids, 2004. - Vol. 46. - pp. 127-162. - DOI: 10.1002/flid.748.

Lim E. [et al.] Digital Elevation Models of Pago Pago, American Samoa: Procedures, Data Sources and Analysis [Online] // Tsunami Inundation Gridding Project | ngdc.noaa.gov. - 2009. –

http://www.ngdc.noaa.gov/mgg/inundation/tsunami/data/pago_pago_as/pago_pago_as.pdf.

Mader C. Numerical modeling of water waves [Book]. - [s.l.] : CRC Press, 2004. - ISBN 0-8493-2311-8.

Marche F. Theoretical and Numerical Study of Shallow Water Models. Applications to Nearshore Hydrodynamics. [Online]. - PhD Thesis; Université de Bordeaux, 2005. –

http://www.math.u-bordeaux.fr/~marche/THESE_Marche.pdf.

OCHA Samoa-Tonga Tsunami OCHA Situation Report No. 6 [Online] // ReliefWeb. - 6 October 2009. –

<http://www.reliefweb.int/rw/rwb.nsf/db900sid/AZHU-7WL2CX?OpenDocument>.

Okada Y. Surface deformation due to shear and tensile faults in a half-space [Article] // Bulletin of the Seismological Society of America.. - 1985. - Vol. 75. - pp. 1135-1154.

Pararas-Carayannis G. and Dong B. CATALOG OF TSUNAMIS IN THE SAMOA ISLANDS [Online] // <http://www.drgeorgepc.com/TsunamiSamoaIslandsCatalog.pdf>. - 1980.

Pelletier B., Calmant S. and Pillet B. Current tectonics of the Tonga–New Hebrides region [Article] // *Earth and Planetary Science Letters*. - 1998. - Vol. 164. - pp. 263-276.

Titov V.V, and Gonzales F.I. Implementation and testing of Method of Splitting Tsunami (MOST) model [Report] : Technical Memorandum / ERL PMEL ; NOAA. - 1997.

Titov V.V. [et al.] Real-time tsunami forecasting: Challenges and solutions [Article] // *Natural hazards*. - 2005. - Special Issue, U.S. National Tsunami Hazard Mitigation Program : Vol. 35(1). - pp. 41-45.

UNITAR/UNOSAT Tsunami in Samoa Island [Online] // International Space Charter website. - 29 09 2009. - 27 09 2010. - http://www.disasterscharter.org/web/charter/activation_details?p_r_p_1415474252_assetId=ACT-273.

Ward S.N. Tsunamis, *Encyclopedia of Physical Science and Technology* [Book] / ed. Meyers R.A.. - [s.l.] : Academic Press., 2002. - Vol. 17 : pp. 175-191.

Weinstein S. Lundgren P. Finite Fault Modeling in a Tsunami Warning Center Context [Journal]. - [s.l.] : *Pure and Applied Geophysics*, 2008. - Vol. 165. - pp. 451-474. - DOI 10.1007/s00024-008-0316-x.